Pulsed Nuclear Magnetic Resonance in Rotating Solids*

H. KESSEMEIER† AND R. E. NORBERG
Department of Physics, Washington University, St. Louis, Missouri
(Received October 1966)

Pulsed nuclear-magnetic-resonance measurements have been made on rapidly rotating solid samples. Transient induction signals were observed for P^{31} and Al^{27} nuclei in Mg_3P_2, Zn_3P_2, and AlP powders. A stochastic theory of relaxation is used to discuss the transverse and longitudinal spin relaxation processes. Indirect nuclear exchange appears to limit the relaxation times T_1 and T_2 at high rotation rates.

I. INTRODUCTION

THE method of sample rotation was first employed by Andrew, Bradbury, and Eades[1] to demonstrate the invariance of the second moment of a nuclear absorption line upon rotation of the crystal. It was recognized independently by Lowe[2] and Andrew *et al.*[3–5] that this technique can be used in the search for residual nuclear interactions in solids which are, in the static crystal, obscured by a dominant magnetic dipolar coupling. The time-independent part of the truncated dipole-dipole interaction among the nuclei in a rotating solid[2,6–10] contains the angular factor $\lambda(\Theta)=\frac{1}{2}(3\cos^2\Theta-1)$ which can be brought to zero exactly by aligning the axis of rotation at the "magic angle"

$$\Theta=\cos^{-1}(\tfrac{1}{3})^{1/2}=54.7^\circ \qquad (1)$$

with respect to the direction of the applied magnetic field. The remaining two time-dependent terms become arbitrarily small if the specimen is rotated at a frequency Ω large compared to the linewidth of the static crystal, i.e.,

$$\Omega/\sigma\gg 1, \qquad (2)$$

where σ is the root-mean-square second moment of the resonance line shape.

Condition (2) imposes severe limitations upon the effectiveness of this method in narrowing a dipolar-broadened line. In the present investigation, rotational frequencies of up to 8 kc/sec were obtained with a 1-cm-diam rotor. In exceptional cases, 10 kc/sec was reached. At this point, the rim acceleration amounts to about $2\times10^6 g$ (g is the acceleration of gravity) often leading to a complete disintegration of the sample. However, nuclear linewidths in solids of up to 10 kc/sec and beyond are not unusual. For example, $\sigma=10.8$ kc/sec of the F^{19} resonance in a polycrystalline sample of CaF_2. It is therefore an advantage to select solids with a reasonably narrow static linewidth which entails large interatomic distances and small gyromagnetic ratios of the resonant nuclei. Accordingly, the P^{31} resonance in various metal phosphides was chosen which, in Mg_3P_2 and Zn_3P_2, has a static width of about 1 kc/sec.

It should be pointed out that, in general, any rotationally noninvariant interaction in solids will be attenuated by rapid sample rotation.[3,11] The electron coupled nuclear exchange interaction is, however, invariant under rotation and will survive the averaging process. It can therefore be measured, provided conditions (1) and (2) apply.[7]

If spin diffusion contributes to nuclear spin-lattice relaxation, sample rotation is also expected to affect the return of nuclear magnetization to its equilibrium value. According to Bloembergen,[12] the magnetic dipolar interaction transports nuclear Zeeman energy to paramagnetic impurities present in the solid by permitting spin-energy-conserving transitions between neighboring nuclei. The impurity ions serve as links between the nuclear spins in their vicinity and the lattice phonons. If conditions (1) and (2) apply, spin diffusion caused by the dipolar coupling will be quenched by sample rotation. Hence, a careful study of the characteristic longitudinal relaxation time as a function of the spinning frequency may serve as a complementary procedure to line narrowing in detecting residual nuclear interactions in solids.

In Sec. II, the stochastic approach is used in describing nuclear relaxation in a rotating solid assuming the existence of only the magnetic dipolar interaction. Section III is concerned with the apparatus and experimental technique. The results of the measurements are given in Sec. IV, and Sec. V contains a summary of this investigation.

* This work was supported by a grant from the U. S. Air Force Office of Scientific Research, a Frederick Gardner Cottrell Grant from the Research Corporation, and by an Advanced Research Projects Agency Materials Research Equipment Grant.
† Present address: Department of Physics, University of North Carolina, Chapel Hill, North Carolina.
[1] E. R. Andrew, A. Bradbury, and R. G. Eades, Arch. Sci. (Geneva) **11**, 223 (1958); Nature **182**, 1659 (1958).
[2] I. J. Lowe, Phys. Rev. Letters **2**, 285 (1959).
[3] E. R. Andrew, Arch. Sci. (Geneva) **12**, 103 (1959).
[4] E. R. Andrew, A. Bradbury, and R. G. Eades, Nature **183**, 1802 (1959).
[5] E. R. Andrew, A. Bradbury, R. G. Eades, and G. J. Jenks, Compt. Rend. Colloq. Ampere (Pisa) **9**, 371 (1960); Nature **188**, 1096 (1960).
[6] E. R. Andrew and R. A. Newing, Proc. Phys. Soc. (London) **72**, 959 (1958).
[7] J. Dreitlein and H. Kessemeier, Phys. Rev. **123**, 835 (1961).
[8] E. R. Andrew, Compt. Rend. Colloq. Ampere (Leipzig) **10**, 210 (1961).
[9] S. Clough and K. W. Gray, Proc. Phys. Soc. (London) **79**, 457 (1962); **80**, 1382 (1962).
[10] E. R. Andrew and G. J. Jenks, Proc. Phys. Soc. (London) **80**, 663 (1962).
[11] H. Kessemeier, Ph.D. thesis, Washington University, 1964 (unpublished).
[12] N. Bloembergen, Physica **15**, 386 (1949).

II. STOCHASTIC THEORY OF RELAXATION PROCESSES IN A ROTATING SOLID

A. Transverse Relaxation

A system of nuclear spins regularly disposed at lattice sites of a crystalline solid in an external magnetic field and interacting among themselves via spin-dependent forces constitutes a many-body system. A closed form solution of the line-shape problem of such a system has not been derived on the basis of a rigorous quantum-mechanical calculation, although it may be approximated in principle to any degree of accuracy by the the calculable moments of the resonance absorption line.[13–15] If the solid is mechanically rotated, the Hamiltonian of the system depends on time explicitly and, in general, does not commute with itself at different times. Again, however, the second and fourth moments of the line can be evaluated.[7]

The interaction among the nuclear spins is assumed to be purely dipolar with magnitude small compared to the coupling strength of the nuclear moments with the applied uniform field $H_0\hat{z}$. The Hamiltonian of a system of identical nuclei with gyromagnetic ratio γ may then be written

$$\mathcal{H}(t)=\mathcal{H}_Z+G(t), \tag{3}$$

where the dipolar energy $G(t)$ is considered as a perturbation of the Zeeman term $\mathcal{H}_Z=-\gamma\hbar H_0\sum_j I_j^z$. In general, $G(t)$ may be decomposed into the form[16]

$$G(t)=\sum_{l=-2}^{2} G^l(t)=\sum_{j,k}\sum_{l=-2}^{2}(1-\delta_{jk})U_{jk}{}^l(t)V_{jk}{}^l. \tag{4}$$

The $U_{jk}{}^l(t)$ depend on the spatial coordinates of the internuclear vector $\mathbf{r}_{jk}(t)$ as

$$U_{jk}{}^l(t)=(3\pi/10)^{1/2}\gamma^2\hbar^2 r_{jk}{}^{-3}(-1)^l \times Y_2{}^{-l}[\vartheta_{jk}(t),\varphi_{jk}(t)], \tag{5}$$

and the $V_{jk}{}^l$ are defined in terms of the spin operators

$$V_{jk}{}^0=-(8/3)^{1/2}[I_j{}^0I_k{}^0-\tfrac{1}{4}(I_j{}^{+1}I_k{}^{-1}+I_j{}^{-1}I_k{}^{+1})], \tag{6a}$$

$$V_{jk}{}^{\pm1}=\pm(I_j{}^0I_k{}^{\pm1}+I_j{}^{\pm1}I_k{}^0), \tag{6b}$$

$$V_{jk}{}^{\pm2}=-I_j{}^{\pm1}I_k{}^{\pm1}, \tag{6c}$$

where $I_j{}^0=I_j{}^z$ and $I_j{}^{\pm1}=I_j{}^x\pm iI_j{}^y$. The $Y_2{}^l[\vartheta_{jk}(t),\varphi_{jk}(t)]$ are normalized spherical harmonics defined as

$$Y_2{}^0[\vartheta_{jk}(t),\varphi_{jk}(t)]=-(5/16\pi)^{1/2}\times[1-3\cos^2\vartheta_{jk}(t)], \tag{7a}$$

$$Y_2{}^{\pm1}[\vartheta_{jk}(t),\varphi_{jk}(t)]=\mp(15/8\pi)^{1/2}\cos\vartheta_{jk}(t)\times\sin\vartheta_{jk}(t)e^{\pm i\varphi_{jk}(t)}, \tag{7b}$$

$$Y_2{}^{\pm2}[\vartheta_{jk}(t),\varphi_{jk}(t)]=(15/32\pi)^{1/2}\sin^2\vartheta_{jk}(t)e^{\pm2i\varphi_{jk}(t)}. \tag{7c}$$

One needs the explicit time dependence of the angular factors of the interparticle unit vecor $\hat{r}_{jk}(t)$ in (7). To this end a coordinate transformation is performed from the laboratory frame $[\vartheta_{jk}(t),\varphi_{jk}(t)]$ in which the applied magnetic field points along the z axis to a frame $[\vartheta_{jk}',(\varphi_{jk}'+\Omega t)]$ in which the axis of rotation chosen along $\hat{z}'$ is the polar axis. If the sample is rotated at frequency Ω about this axis inclined at angle Θ with respect to $H_0\hat{z}$, it is found with reference to Fig. 1,

$$1-3\cos^2\vartheta_{jk}(t)=-\tfrac{1}{2}(1-3\cos^2\Theta)(1-3\cos^2\vartheta_{jk}') -\tfrac{3}{2}\sin2\Theta\sin2\vartheta_{jk}'\cos(\Omega t+\varphi_{jk}')-\tfrac{3}{2}\sin^2\Theta\sin^2\vartheta_{jk}'\cos2(\Omega t+\varphi_{jk}'), \tag{8a}$$

$$\sin\vartheta_{jk}(t)\cos\vartheta_{jk}(t)e^{\pm i\varphi_{jk}(t)}=-\tfrac{1}{2}\sin2\Theta(1-\tfrac{3}{2}\sin^2\vartheta_{jk}') +\tfrac{1}{2}\cos2\Theta\sin2\vartheta_{jk}'\cos(\Omega t+\varphi_{jk}')+\tfrac{1}{4}\sin2\Theta\sin^2\vartheta_{jk}'\cos2(\Omega t+\varphi_{jk}') \pm\binom{i}{2}[\cos\Theta\sin2\vartheta_{jk}'\sin(\Omega t+\varphi_{jk}')+\sin\Theta\sin^2\vartheta_{jk}'\sin2(\Omega t+\varphi_{jk}')], \tag{8b}$$

$$\sin^2\vartheta_{jk}(t)e^{\pm2i\varphi_{jk}(t)}=\sin^2\Theta(1-\tfrac{3}{2}\sin^2\vartheta_{jk}') -\tfrac{1}{2}\sin2\Theta\sin2\vartheta_{jk}'\cos(\Omega t+\varphi_{jk}')+\tfrac{1}{2}(1+\cos^2\Theta)\sin^2\vartheta_{jk}'\cos2(\Omega t+\varphi_{jk}') \pm i[-\sin\Theta\sin2\vartheta_{jk}'\sin(\Omega t+\varphi_{jk}')+\cos\Theta\sin^2\vartheta_{jk}'\sin2(\Omega t+\varphi_{jk}')]. \tag{8c}$$

In a calculation of the nuclear resonance line shape in a static or rotating solid (for $\Omega\ll\gamma H_0$) only the secular term $G^0(t)$ of the magnetic dipole-dipole interaction (4) has to be retained since it commutes with the dominant Zeeman term $\mathcal{H}_z$. The nonsecular terms $G^l(t)$ with $l\neq0$ are of importance in the exchange of nuclear Zeeman energy at impurity sites of the crystal via a direct dipolar coupling between paramagnetic electrons and neighboring nuclear spins.

In the semiclassical treatment of the line-shape problem, matrix elements involving spin-energy–conserving transitions between states of the nuclear system as generated by the truncated magnetic dipolar interaction $G^0(t)$ are replaced by random functions of time.

[13] J. H. Van Vleck, Phys. Rev. **74**, 1168 (1948).
[14] R. Kubo and K. Tomita, J. Phys. Soc. Japan **9**, 888 (1954).
[15] I. J. Lowe and R. E. Norberg, Phys. Rev. **107**, 46 (1957).
[16] P. S. Hubbard, Rev. Mod. Phys. **33**, 249 (1961).

It is assumed that all spins are equivalent and experience a stationary random local field having a Gaussian probability distribution. A correlation function $\langle\Delta\omega(t)\Delta\omega(t-\tau)\rangle$ is introduced which describes the time-averaged fluctuations of the local field $\Delta\omega(t)$ at a typical lattice site.

In terms of this correlation function, Anderson[17] derived an expression for the normalized free induction decay of the nuclear signal which is related to the resonance absorption line by a Fourier transformation[14,15] and is directly observed experimentally.

$$\Phi(t)=\exp\left[-\int_0^t(t-\tau)\langle\Delta\omega(t)\Delta\omega(t-\tau)\rangle d\tau\right], \quad (9)$$

where the angular bracket signifies the time average.

This result has been used by Clough and Gray[9] to calculate line-shape changes caused by rapid rotation of a solid. In a calculation of this type two major simplifications of the more general problem of random motional narrowing arise. First, only the spherical angles of the internuclear vector become time-dependent while its magnitude remains fixed in time. Second, the frequency distribution of internal nuclear motion reduces to a single frequency, the rate of rotation of the solid.

The nuclear dipolar local field $\Delta\omega(t)$ at a typical lattice site for a rigid crystalline solid rotating at frequency Ω about an axis inclined at angle Θ to $H_0\hat{z}$ then has to be evaluated. It will depend upon the orientation of the internuclear as well as the spin vectors and, with (8a), is given by

$$\Delta\omega(t)=\sum_k A_{jk}(t)[1-3\cos^2\vartheta_{jk}(t)]$$
$$=\sum_k A_{jk}(t)[a_{jk}\lambda(\Theta)+b_{jk}\cos(\Omega t+\varphi_{jk}')+c_{jk}\cos 2(\Omega t+\varphi_{jk}')], \quad (10)$$

where

$$a_{jk}=1-3\cos^2\vartheta_{jk}'; \quad b_{jk}=-\tfrac{3}{2}\sin 2\Theta\sin 2\vartheta_{jk}';$$
$$c_{jk}=-\tfrac{3}{2}\sin^2\Theta\sin^2\vartheta_{jk}';$$
$$\lambda(\Theta)=\tfrac{1}{2}(3\cos^2\Theta-1) \quad \text{with} \quad -\tfrac{1}{2}\leq\lambda(\Theta)\leq 1.$$

The coefficients $A_{jk}(t)$ depend on the orientation of the spin vectors. They carry a time dependence because $G^0(t)$ generates random and uncorrelated transitions among the nuclear spins. Since the second moment $\langle\Delta\omega^2(t)\rangle=\sigma^2$ of the resonance absorption line is invariant under rotation,[1,18] these coefficients are defined by

$$\left\langle\sum_k A_{jk}^2(t)[1-3\cos^2\vartheta_{jk}(t)]^2\right\rangle=\sigma^2. \quad (11)$$

As long as the spinning frequency Ω is small compared to the nuclear Larmor precession, spin transitions induced by mechanical rotation of the solid are negligible.[19] In evaluating the stationary random correlation function $\langle\Delta\omega(t)\Delta\omega(t-\tau)\rangle$, the time average may then be carried out independently over quantities determining the orientations of the internuclear and the spin vectors, and the only contributing terms are

$$\langle\Delta\omega(t)\Delta\omega(t-\tau)\rangle=\left\langle\sum_k A_{jk}(t)A_{jk}(t-\tau)\{a_{jk}^2\lambda^2(\Theta)\right.$$
$$+b_{jk}^2\cos[\Omega t+\varphi_{jk}']\cos[\Omega(t-\tau)+\varphi_{jk}']$$
$$\left.+c_{jk}^2\cos 2[\Omega t+\varphi_{jk}']\cos 2[\Omega(t-\tau)+\varphi_{jk}']\}\right\rangle. \quad (12)$$

It will be assumed that the time dependence of the interaction between any pair of nuclear spins may be described adequately by an exponential correlation function depending upon a single correlation time τ_c. This correlation time is a measure of the average lifetime of a typical spin between two transitions as generated by $G^0(t)$. Then, with (11) one has

$$\left\langle\sum_k A_{jk}(t)A_{jk}(t-\tau)\right\rangle=(5/4)\sigma^2e^{-\tau/\tau_c}. \quad (13)$$

Carrying out the time average over the orientations of the internuclear vectors and replacing the quantities a_{jk}, b_{jk}, and c_{jk} by their uniform angular averages (all measurements have been performed on powdered samples)

$$\langle a_{jk}^2\rangle_{\rm av}=4/5; \quad \langle b_{jk}^2\rangle_{\rm av}=(6/5)\sin^2 2\Theta;$$
$$\langle c_{jk}^2\rangle_{\rm av}=(6/5)\sin^4\Theta$$

yields

$$\langle\Delta\omega(t)\Delta\omega(t-\tau)\rangle=\sigma^2e^{-\tau/\tau_c}[\lambda^2(\Theta)+\tfrac{3}{4}\sin^2 2\Theta\cos\Omega\tau$$
$$+\tfrac{3}{4}\sin^4\Theta\cos 2\Omega\tau]. \quad (14)$$

The free induction decay $\Phi_\Omega(t)$ of a solid rotating at frequency Ω is then immediately obtained from (9) and

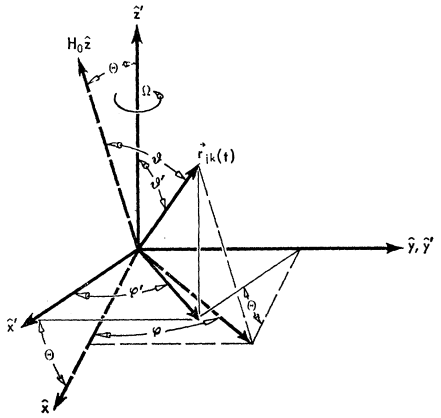

FIG. 1. The orientation of the applied magnetic field $H_0\hat{z}$ and the internuclear vector $\mathbf{r}_{jk}(t)$ relative to the axis of rotation directed along $\hat{z}'$.

[17] P. W. Anderson, J. Phys. Soc. Japan **9**, 316 (1954).
[18] G. E. Pake, in *Solid State Physics*, edited by F. Seitz and D. Turnbull (Academic Press Inc., New York, 1956), Vol. 2, p. 46.
[19] S. P. Heims and E. T. Jaynes, Rev. Mod. Phys. **34**, 143 (1962).

(14), which yield

$$\Phi_\Omega(t)=\exp\{-\sigma^2\tau_c^2[e^{-t/\tau_c}-1+t/\tau_c]\lambda^2(\Theta)$$
$$-\tfrac{3}{4}\sigma^2\sin^2 2\Theta[\tau_c t[1+(\Omega\tau_c)^2]^{-1}+\tau_c^2[1+(\Omega\tau_c)^2]^{-2}$$
$$\times\{[1-(\Omega\tau_c)^2][e^{-t/\tau_c}\cos\Omega t-1]-2\Omega\tau_c e^{-t/\tau_c}\sin\Omega t\}]$$
$$-\tfrac{3}{4}\sigma^2\sin^4\Theta[\tau_c t[1+(2\Omega\tau_c)^2]^{-1}+\tau_c^2[1+(2\Omega\tau_c)^2]^{-2}$$
$$\times\{[1-(2\Omega\tau_c)^2][e^{-t/\tau_c}\cos 2\Omega t-1]$$
$$-4\Omega\tau_c e^{-t/\tau_c}\sin 2\Omega t\}]\}. \quad (15)$$

For $\Theta=0$, $\Phi_\Omega(t)$ becomes independent of Ω and reduces to the well-known relaxation function which describes the transformation of the line shape from a rigid lattice Gaussian to a Lorentzian in the case of extreme narrowing, depending on the magnitude of $\sigma\tau_c$.[14,20,21] The same result may be obtained by letting Ω become sufficiently large

$$\Phi_{\Omega\to\infty}(t)=\exp\{-\sigma^2\tau_c^2[e^{-t/\tau_c}-1+t/\tau_c]\lambda^2(\Theta)\}, \quad (16)$$

except that in this case the free induction decay contains the externally adjustable parameter $\lambda^2(\Theta)$ which, from (10), may be varied continuously between 0 and 1.

It follows from (15) and (16) that for high spinning frequencies Ω an effective reduction of the dipolar coupling strength between the nuclear moments can only be achieved if the angle Θ between the axis of rotation and the direction of the applied magnetic field is chosen in such a way that $\lambda(\Theta)\equiv 0$, which implies from (10)

$$\Theta=\cos^{-1}(\tfrac{1}{3})^{1/2}=54.7^\circ. \quad (17)$$

All experimental data taken have been obtained by carefully adjusting the spinning axis to this "magic angle."

In the following, condition (17) will therefore always be invoked.

Line-shape changes caused by sample rotation frequencies $\Omega/\sigma\gtrsim 1$ are of primary interest. Since the rigid lattice limit implies $\sigma\tau_c\gg 1$, it may safely be assumed that $\Omega\tau_c\gg 1$. With this condition, the terms in (15) containing $\sin\Omega t$ and $\sin 2\Omega t$ may be neglected because they are reduced in magnitude by a factor of $1/\Omega\tau_c$ as compared to the terms multiplied by $\cos\Omega t$ and $\cos 2\Omega t$. For rapid rotation at the magic angle, (15) then reduces to

$$\Phi_\Omega(t)=\exp\{-t/T_2(\Omega)$$
$$-\tfrac{3}{4}(\sigma/\Omega)^2[1-\tfrac{1}{9}(8\cos\Omega t+\cos 2\Omega t)e^{-t/\tau_c}]\}$$
$$(\sigma/\Omega\lesssim 1, \Omega\tau_c\gg 1), \quad (18)$$

where $t\gtrsim 0$ and the transverse relaxation time $T_2(\Omega)$ is given by

$$T_2(\Omega)=\tfrac{4}{3}(\Omega\tau_c)^2/\sigma^2\tau_c. \quad (19)$$

The observed free induction decay $\Phi_\Omega(t)$ of the transverse magnetization of a solid specimen rotated at the angle $\Theta=54.7^\circ$ at increasing frequencies Ω thus will undergo a remarkable transformation from a broad Gaussian in the static case to a simple exponential decay with a time constant $T_2(\Omega)$ which is expected to increase proportionally to Ω^2. The transition region between these extreme cases is characterized by a more complicated but calculable relaxation function coherently modulated at a rate given by the spinning frequency. This modulation will decrease in magnitude as $(\sigma/\Omega)^2$. These predictions have been tested experimentally with results reported in Sec. IV.

B. Longitudinal Relaxation

A system of spin $\frac{1}{2}$ nuclei placed in an external magnetic field, strong enough to permit a treatment of the magnetic dipolar coupling as a small perturbation on the Zeeman energy, relaxes to the lattice in insulators and semiconductors via a chain of events.[12] From the point of view of nuclear magnetic resonance, the longitudinal relaxation may be broken up into two distinctly different processes which combine to establish thermal equilibrium of the perturbed nuclear spin system with the lattice which acts as a heat reservoir at a given temperature. The truncated magnetic dipolar coupling among the nuclear moments permits energy to diffuse through the nuclear-spin system via spin-energy-conserving transitions. The contact between the nuclei and the lattice is provided by paramagnetic impurities present in the sample which are coupled to the various modes of lattice vibrations and interact with the nuclear spins in their immediate vicinity via a magnetic dipole-dipole coupling.

The time rate of change of the nuclear spin magnetization density $\rho_z(r,t)$ will hence depend upon a spin diffusion term $(\partial\rho/\partial t)_D$ and a relaxation term $(\partial\rho/\partial t)_R$ and may be written as

$$\frac{\partial}{\partial t}\rho(r,t)=\left(\frac{\partial\rho}{\partial t}\right)_D+\left(\frac{\partial\rho}{\partial t}\right)_R$$
$$=D\nabla^2\rho(r,t)-C[\rho(r,t)-\rho_0]\sum_n|\mathbf{r}-\mathbf{r}_n|^{-6}. \quad (20)$$

Here, ρ_z represents the thermal equilibrium nuclear polarization density, $\mathbf{r}_n$ indicates the position of the nth impurity site, D is the diffusion coefficient, and C is a coupling strength parameter between an impurity ion and a nuclear spin in its vicinity.

The total magnetization of the nuclear system then varies as

$$M_z(t)=\int\rho(r,t)d^3r, \quad (21)$$

where the volume integral has to be carried out over the entire crystal excluding the nuclei within the "sphere of influence" around each paramagnetic impurity. These nuclei do not contribute to the resonance signal being shifted in frequency by the action of the large electronic moment of the impurity ion.

[20] A. Abragam, *The Principles of Nuclear Magnetism* (Oxford University Press, London, 1961), p. 433.
[21] M. Bloom and H. S. Sandhu, Can. J. Phys. **40**, 292 (1962).

In the absence of a formal theory of spin diffusion, a model is adopted in which the nuclei within a sphere of radius R_c around each impurity relax to the lattice via a direct dipolar coupling with the ion. At a nuclear site with $|\mathbf{r}-\mathbf{r}_n|<R_c$ the contribution of the dipolar local field arising from all nearest-neighboring nuclear spins is assumed to be negligible as compared to the field produced by the randomly fluctuating impurity spin. Thus, the nuclei in this region are removed from the resonance line and, since $G^0(t)$ permits only energy-conserving mutual spin flips, spin diffusion will be quenched for $|\mathbf{r}-\mathbf{r}_n|<R_c$.

R_c has been defined by Blumberg[22] as that distance from the isolated impurity at which the magnetic dipolar field of the paramagnetic ion is equal to the nuclear linewidth. Khutsishvili[23] and Rorschach[24] have estimated the order of magnitude of R_c by equating the change of the effective ionic dipole field over one lattice spacing with the local nuclear dipolar field. These definitions of the diffusion barrier radius make it independent of sample rotation.

The dependence of C and D on sample rotation will now be examined. If the concentration of paramagnetic impurities in the host lattice is small, a paramagnetic ion can be considered as isolated from other impurities. The ion is tightly coupled to the lattice phonons via the spin-orbit interaction and, as a result, suffers frequent and irregular transitions which produce a rapidly fluctuating magnetic field in its vicinity inducing, in turn, transitions among the various states of the nuclear spins located at neighboring sites through the magnetic dipolar coupling.

As far as nuclear relaxation is concerned, it suffices to consider only the z component of the impurity spin and to attach a time dependence to S^z representing its coupling to the lattice such that the time average of its correlation function is given by

$$\langle S^z(t)S^z(t-\tau)\rangle=\tfrac{1}{3}S(S+1)e^{-\tau/\tau_e}, \tag{22}$$

where τ_e is the electronic relaxation time which, in general, depends on temperature and the applied magnetic field.

The Hamiltonian of the electron-nuclear system then may be written

$$\mathcal{H}_{n-e}(t)=\mathcal{H}_z+G_j^{(1)}(t), \tag{23}$$

where $\mathcal{H}_z=-\hbar H_0(\gamma_S S^z+\gamma_I I_j^z)$ is the Zeeman part and, from (4)

$$G_j^{(1)}(t)=-\tfrac{3}{2}\gamma_S\gamma_I\hbar^2 r_j^{-3}\sin\vartheta_j\cos\vartheta_j \times(e^{-i\varphi_j}I_j^{+}+e^{i\varphi_j}I_j^{-})S^z(t) \tag{24}$$

represents the interaction Hamiltonian of the two-body problem. $G_j^{(1)}(t)$ produces spin flips of the jth nucleus unaccompanied by electronic transitions and is assumed to dominate nuclear relaxation near the impurity site. Here, r_j is the distance to the jth nucleus as measured from the paramagnetic ion, ϑ_j and φ_j are the spherical angles of this vector (Fig. 1) and γ_S and γ_I are the gyromagnetic ratios of the ion and the nucleus, respectively.

With (24), the transition probability $W(r_j,H_0)$, of a nucleus at a distance r_j from the impurity ion is determined by[12,20]

$$W(r_j,H_0)=C(H_0)r_j^{-6}=3\gamma_S^2\gamma_I^2\hbar^2 r_j^{-6}S(S+1) \times\sin^2\vartheta_j\cos^2\vartheta_j\tau_e[1+(\omega_I\tau_e)^2]^{-1}, \tag{25}$$

where $\omega_I=\gamma_I H_0$ is the nuclear Larmor frequency and the coupling strength parameter $C(H_0)$ is independent of the distance of the nucleus from the impurity center.

It the crystal is rotated at frequency Ω, the angles ϑ_j and φ_j of the electron-nuclear vector in (24) will explicitly depend on time. Applying transformation (8b) to (24), the transition probability of a nucleus in the vicinity of an impurity is then found to be

$$\begin{aligned}W(r_j,H_0,\Omega)&=C(H_0,\Omega)r_j^{-6}=\tfrac{3}{16}\gamma_S^2\gamma_I^2\hbar^2 r_j^{-6}S(S+1)\tau_e\\&\times\{4\sin^2 2\Theta(1-\tfrac{3}{2}\sin^2\vartheta_j')^2[1+\omega_I^2\tau_e^2]^{-1}\\&+(\cos^2\Theta+\cos^2 2\Theta)\sin^2 2\vartheta_j'([1+(\omega_I+\Omega)^2\tau_e^2]^{-1}\\&+[1+(\omega_I-\Omega)^2\tau_e^2]^{-1})+(\sin^2\Theta+\tfrac{1}{4}\sin^2 2\Theta)\sin^4\vartheta_j'\\&\times([1+(\omega_I+2\Omega)^2\tau_e^2]^{-1}+[1+(\omega_I-2\Omega)^2\tau_e^2]^{-1})\}.\end{aligned} \tag{26}$$

It follows from (26) that this nuclear transition rate is modified to order Ω/ω_I by sample rotation. Thus, the dipolar coupling strength parameter $C(H_0)$ is not affected by mechanical rotation of the solid under present experimental conditions ($\Omega/\omega_I<10^{-3}$), i.e.,

$$C(H_0,\Omega)=C(H_0)[1+O(\Omega/\omega_I)]. \tag{27}$$

This result is not surprising since nuclear Zeeman energy $\hbar\omega_I$ is exchanged at the impurity sites while the spinning frequency Ω is of the order of the static nuclear linewidth $\Delta\omega_I$. The diffusion coefficient D in (20), on the other hand, is associated with mutual nuclear spin-flips in which an exchange of energy $\hbar\Delta\omega_I$ occurs. In this case, rotational frequencies $\Omega\approx\Delta\omega_I$ are expected to play an important role.

The part of the magnetic dipole-dipole interaction responsible for energy conserving mutual spin flips of neighboring nuclei and thus for nuclear spin diffusion from (4) is given by

$$G^{(0)}(t)=\sum_{j<k}-\tfrac{1}{4}\gamma_I^2\hbar^2 r_{jk}^{-3}[I_j^{+}I_k^{-}+I_j^{-}I_k^{+}] \times(1-3\cos^2\vartheta_{jk}(t)), \tag{28}$$

where the angular factor $[1-3\cos^2\vartheta_{jk}(t)]$ may be expanded in the rotating coordinate system as in (8a) and (10).

The many-particle spin system is reduced to a two-body system by lumping the effect on the jth spin of all

[22] W. E. Blumberg, Phys. Rev. **119**, 79 (1960).
[23] G. R. Khutsishvili, Zh. Eksperim. i Teor. Fiz. **42**, 1311 (1962) [English transl.: Soviet Phys.—JETP **15**, 909 (1962)].
[24] H. E. Rorschach, Jr., Physica **30**, 38 (1964).

other nuclear spins but the kth spin into an effective local field giving rise to a Larmor frequency $\omega_I-\Delta\omega_j$ for the jth spin. Similarly, the frequency deviation of the kth spin from the Larmor precession of an isolated nuclear moment is $\omega_I-\Delta\omega_k$. The distributions of $\Delta\omega_j$ and $\Delta\omega_k$ are assumed to be represented by the line-shape function $I(\omega)$. The transition probability per unit time of a mutual spin-flip between the jth and kth nuclear spin induced by $G^{(0)}(t)$ and averaged over the Larmor frequency distribution is then obtained

$$W_{jk}(\Theta,\Omega)=\tfrac{1}{8}\pi\gamma_I{}^4\hbar^2r_{jk}{}^{-6}\Big[\lambda^2(\Theta)a_{jk}{}^2\int_{-\infty}^{\infty}I^2(\omega)d\omega+\tfrac{1}{2}b_{jk}{}^2\int_{-\infty}^{\infty}I(\omega)I(\omega+\Omega)d\omega+\tfrac{1}{2}c_{jk}{}^2\int_{-\infty}^{\infty}I(\omega)I(\omega+2\Omega)d\omega\Big], \quad (29)$$

where $\lambda(\Theta)$, a_{jk}, b_{jk}, and c_{jk} are given by (10).

Experimentally, the free induction decay $\Phi_\Omega(t)$ is observed. It has been shown[14,15] that in the high-temperature approximation (for temperatures above 10^{-3} °K for a nuclear spin system in an applied magnetic field of 10^4 G) the spectral line function $I(\omega)$ is the Fourier transform of $\Phi_\Omega(t)$

$$I(\omega)=(2\pi)^{-1/2}\int_{-\infty}^{\infty}e^{i\omega t}\Phi_\Omega(t)dt. \quad (30)$$

This relation permits expressing $W_{jk}(\Theta,\Omega)$ in terms of integrals over Bloch decay functions.

The total transition rate $W(\Theta,\Omega)$ of the jth nuclear spin in a rotating solid is obtained by averaging over all nearest neighbors. It is again assumed that the angular part of this average is adequately represented by a uniform angular average and $r_{jk}{}^6$ is replaced by an average $\langle r_{jk}{}^6\rangle_{\rm av}$ over nearest neighbors. With (30), (29) then becomes

$$W(\Theta,\Omega)=\tfrac{1}{8}\pi\gamma_I{}^4\hbar^2\langle r_{jk}{}^6\rangle_{\rm av}{}^{-1}\Phi_\Omega{}^{-2}(0)\times\Big[\lambda^2(\Theta)\langle a_{jk}{}^2\rangle_{\rm av}\int_{-\infty}^{\infty}\Phi_\Omega{}^2(t)dt+\tfrac{1}{2}\langle b_{jk}{}^2\rangle_{\rm av}\int_{-\infty}^{\infty}\Phi_\Omega{}^2(t)e^{i\Omega t}dt+\tfrac{1}{2}\langle c_{jk}{}^2\rangle_{\rm av}\int_{-\infty}^{\infty}\Phi_\Omega{}^2(t)e^{2i\Omega t}dt\Big], \quad (31)$$

where $\langle a_{jk}{}^2\rangle_{\rm av}$, $\langle b_{jk}{}^2\rangle_{\rm av}$ and $\langle c_{jk}{}^2\rangle_{\rm av}$ are given by (14).

The integrals appearing in (31) may be evaluated by using the free induction decay $\Phi_\Omega(t)$ from (18). This has been done for sample rotation at the magic angle $\lambda(\Theta)=0$ and high spinning frequencies $\sigma/\Omega\lesssim1$. Only the real part of the integrals in (31) need be retained since $\Phi_\Omega(t)$ is an even function of time. The normalized transition rate $W(\Omega)/W(0)$ is expressed in terms of a power-series expansion in σ/Ω carried out to fourth order. A straightforward but somewhat lengthy calculation yields for $\sigma/\Omega\lesssim1$ and $\Omega\tau_c\gg1$

$$\begin{aligned}D(\Omega)/D(0)&=\tfrac{1}{3}\pi^{-1/2}\sigma T_2(\Omega)\exp(-\tfrac{3}{2}\sigma^2/\Omega^2)[2[1+(\tfrac{1}{2}\alpha)^2]^{-1}\\&+[1+\alpha^2]^{-1}+(1/12)(\sigma/\Omega)^2\{17+10[1+(\tfrac{1}{2}\alpha)^2]^{-1}\\&+16[1+\alpha^2]^{-1}+10[1+(\tfrac{3}{2}\alpha)^2]^{-1}+[1+(2\alpha)^2]^{-1}\}\\&+(1/288)(\sigma/\Omega)^4\{96+420[1+(\tfrac{1}{2}\alpha)^2]^{-1}\\&+195[1+\alpha^2]^{-1}+146[1+(\tfrac{3}{2}\alpha)^2]^{-1}+96[1+(2\alpha)^2]^{-1}\\&+18[1+(\tfrac{5}{2}\alpha)^2]^{-1}+[1+(3\alpha)^2]^{-1}\}], \quad (32)\end{aligned}$$

where $\alpha=\Omega T_2(\Omega)$ and, by definition, the diffusion coefficient $D(\Omega)=a^2W(\Omega)$ with a being the lattice spacing.

The normalized diffusion coefficient (32) has been plotted as the dashed curve in Fig. 11 for the P^{31} longitudinal relaxation in Mg_3P_2 as a function of Ω using (37) and the experimentally measured values of σ and $T_2(\Omega)$. The theoretical curve indicates that spin diffusion caused by the dipolar coupling should have been effectively quenched for high Ω.

The partial differential equation (20) which describes impurity relaxation of nuclear spins in a solid has been solved by several authors.[12,22–26] Under the assumptions that R_c is small compared to the separation of any two impurities and that spherical symmetry exists around each paramagnetic ion, Rorschach[24] has demonstrated that the return of nuclear magnetization $M_z(t)$ to its equilibrium value M_0 for a sufficiently long time after saturation approaches an exponential function of time

$$\frac{\partial}{\partial t}M_z(t)=-\frac{1}{T_1(H_0,\Omega)}[M_z(t)-M_0] \quad (33)$$

with a characteristic time constant

$$1/T_1(H_0,\Omega)=\tfrac{1}{3}8\pi\eta C^{1/4}(H_0)D^{3/4}(\Omega)I_{3/4}(\delta)/I_{-3/4}(\delta), \quad (34)$$

where η is the impurity density and $I_m(\delta)=i^{-m}J_m(i\delta)$ is the hyperbolic Bessel function with $\delta=\frac{1}{2}R_c{}^{-2}(H_0)\times[C(H_0)/D(\Omega)]^{1/2}$.

Relation (34) has two asymptotic limits depending on the magnitude of δ: (1) Rapid spin diffusion ($D\gg C$), i.e., $\delta\ll1$. In this case, $I_m(\delta)$ may be expanded as $I_m(\delta)\cong[1/\Gamma(m+1)](\delta/2)^m$ and (34) reduces to

$$1/T_1(H_0)=\tfrac{1}{3}4\pi\eta C(H_0)/R_c{}^3(H_0). \quad (35)$$

(2) Diffusion-limited relaxation ($D\ll C$), i.e., $\delta\gg1$. In this case, $I_m(\delta)\cong I_{-m}(\delta)$ and (34) simplifies to

$$1/T_1(H_0,\Omega)=\tfrac{1}{3}8\pi\eta C^{1/4}(H_0)D^{3/4}(\Omega). \quad (36)$$

[25] G. R. Khutsishvili, Tr. Inst. Fiz. Akad. Nauk Gruz. SSR 2, 115 (1954); 4, 3 (1956).
[26] P. G. de Gennes, J. Phys. Chem. Solids 7, 345 (1958).

In general, the longitudinal relaxation time $T_1(H_0,\Omega)$ will, therefore, depend on the frequency Ω of sample rotation such that $T_1(H_0,\Omega)$ increases for increasing Ω. Knowing $T_1(H_0,0)$, it is possible to predict the value of $T_1(H_0,\Omega)$ for any Ω with $\sigma/\Omega \lesssim 1$.

In the limit of rapid diffusion (35), in which the bottleneck of nuclear relaxation is at the impurity sites, T_1 appears to be independent of Ω. Since the dipolar diffusion coefficient can be made arbitrarily small for sufficiently large Ω, however, it should always be possible to realize a situation of diffusion-limited relaxation in which nuclear Zeeman energy is transferred to the lattice faster than can be supplied by spin diffusion. In this case, from (36)

$$T_1(H_0,\Omega)/T_1(H_0,0)=[D(0)/D(\Omega)]^{3/4}. \quad (37)$$

This relation permits a direct measurement of the coefficient of spin diffusion independent of the relaxation mechanism at the impurity sites. The experimental results are reported in Sec. IV.

III. EXPERIMENTAL APPARATUS AND PROCEDURE

A. Pulsed NMR Equipment

A standard spin-echo apparatus[27] was operated at 15.9 and 29.0 Mc/sec to observe the free induction decay $\Phi_\Omega(t)$ of magnetization in the plane perpendicular to the direction of the static uniform magnetic field $H_0\hat{z}$. Tektronix 160 series pulsers were used to gate a PG-650C Arenberg oscillator which produced a phase-incoherent rf field of about 14 G in the transmitter coil. A 90° nutation of P^{31} nuclei was achieved in about 10 μsec. A crossed-coil arrangement with electrostatic shielding isolated the signal amplifier from the rf pulse. The amplifiers used were Linear Equipment Laboratories i.f. strips modified to center frequencies of 15.9 and 29.0 Mc/sec. The detected output of the signal amplifier was displayed on a Tektronix 555 oscilloscope. The dc magnetic field required was provided by a Spectromagnetic Industries L12-A2 electromagnet. Varian K-3519 current shims energized by a 6-V storage battery served to improve the field homogeneity across the sample. These shims were not available while the data on Zn_3P_2 were taken.

B. Rotor Sample

In order to contain the powder samples at high rotational frequencies, a spinner shell made of Nylon or Delrin was prepared as shown in Fig. 2. In the process of machining one of these sample containers from a rod of thermoplastic material, a trepanning tool was employed, leaving a bearing and an outer wall of 1-mm thickness.

The powdered sample was mixed with epoxy resin and centrifuged into the partially hollow cylinder which, initially, had a length of about 16 mm. In this process a partial separation of the mixture took place. The sample material was collected at the bottom of the shell while transparent epoxy resin remained at the top. Experiments have shown that the filling factor does not increase if the sample material is tightly packed into the container without the use of epoxy resin.

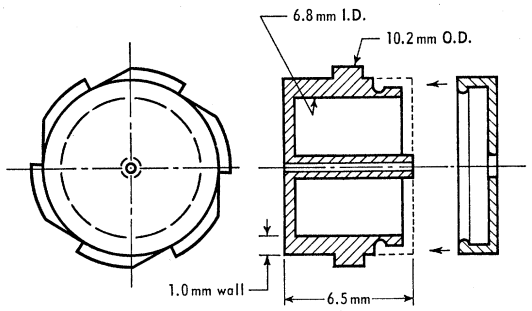

FIG. 2. Rotor sample.

Once the resin is hardened, the filled spinner shell was cut to the actual rotor size and closed with a lid. A snap-in design was employed which permitted a snug mechanical seal of the container without the use of any form of glue. Apart from the lid, the rotor then consisted of a single piece shell equipped with six fins and containing the polycrystalline sample which occupied an effective volume of 0.18 cm^3. It had a diameter of 10.2 mm and was 6.5 mm wide. Experiments indicated that for the spinner to run satisfactorily the ratio of width to diameter should be smaller than one.

The rotor was spun on a thin phosphor bronze axle suspended by a Nylon sample holder which fit snugly to a glass jet. The glass tube was attached to a turntable with protractor and connected via a flexible rubber hose to a standard two-stage regulator attached to a high-pressure gas tank. The turntable permitted orientation of the spinner axis in the horizontal plane. In runs not exceeding 4.0 kc/sec the rotor was driven by compressed air or nitrogen. Higher rotation rates could only be achieved by using a helium jet.

The sound produced by the rapidly rotating sample was picked up by a microphone and displayed in a Lissajous figure against a reference signal from a model 200 CD Hewlett-Packard wide-range oscillator the frequency of which is measured with a model 7360 Beckman electronic counter. A convenient check on the rotation frequency was provided by the "spinning beats," which modulate the free induction decay (18).

The suspension of the rotor has a series of eigenfrequencies. As a consequence, below the highest eigenfrequency rotational energy of the revolving sample can be transferred to the suspension resulting in violent vibrations of suspension and rotor and inducing microphonics into the rf system. These stimulated vibrations account for the fact that no data runs at frequencies below 1.4 kc/sec have been taken. Once the

[27] E. L. Hahn, Phys. Rev. 80, 580 (1950).

spinning frequency exceeded the highest eigenfrequency of the suspension, the spinner ran smoothly and at a constant rate. By slightly adjusting the jet pressure, if necessary, the spinning frequency could easily be kept constant within 0.1% over a period of hours. It is estimated that the spinning axis could be aligned at the magic angle (17) with an accuracy of $\pm 0.5°$.

C. Measurement of the Relaxation Times

The longitudinal relaxation times T_1 were determined by saturation recovery measurements. The nuclear magnetization was saturated at time $t=0$ and at time τ a 90° pulse applied to the sample. The resulting nuclear free precession signal was photographed from an oscilloscope trace. The magnitude of the signal is proportional to the z component of the partially recovered spin magnetization $M_z(\tau)$ existing at time τ. For sufficiently long times after saturation, the nuclear spin system has approached a single spin temperature and the relaxation can be described by a simple exponential recovery (33) of the form

$$M_z(\tau)=M_0[1-e^{\tau/T_1(\Omega)}], \tag{38}$$

where M_0 is the equilibrium magnetization. Equation (38) then determines $T_1(\Omega)$.

The time necessary to complete the measurement of the longitudinal relaxation time for a given spinning frequency varied according to the value of $T_1(\Omega)$. The longest $T_1(\Omega)$ recorded in the present experiment amounted to 1560 sec and required a time of measurement of some 10 h. In spite of many rather lengthy runs and a poor signal-to-noise ratio, it is estimated from the reproducibility of the results that the $T_1(\Omega)$ values quoted are correct within an accuracy of measurement of $\pm 15\%$.

The knowledge of the time origin of the free induction decays is of importance in determining the transverse relaxation times $T_2(\Omega)$, particularly if T_2 is comparable to the length of time t_W of the 90° pulse. Since the nuclear spins are dephasing even in the presence of the rf pulse, the beginning of the decay is expected to be located within t_W. The appearance of the spinning beats facilitates such a determination by extrapolation. Within experimental accuracy it was found that the onset of the signals is located between $0.4t_W$ and $0.5t_W$. All data were corrected accordingly. This empirical result is in good agreement with a recent investigation[28] which finds the time origin of the decays to be located exactly at $0.5t_W$. A correction for the nonlinear detector characteristics was determined and applied to the data before analysis.

[28] D. Barnaal and I. J. Lowe, Phys. Rev. Letters **11**, 258 (1963).

IV. EXPERIMENTAL RESULTS AND DISCUSSION

A. Materials Investigated

For a detailed analysis of a solid under rotation the linewidth of the static sample should be appreciably smaller than the largest achievable spinning frequency. This requirement favors small gyromagnetic ratios and large interatomic distances of the nuclei of interest and led to the selection of several metal phosphide compounds. In particular the P^{31} resonances in magnesium phosphide (Mg_3P_2), zinc phosphide (Zn_3P_2), and aluminum phosphide (AlP) as well as the Al^{27} resonance in AlP and metallic aluminum were studied. Quantitative data about the purity of the compounds used were not available. It was established, however, that the presence of Epoxy Resin in the rotor samples did not modify the NMR results.

Mg_3P_2 and Zn_3P_2 may be considered as compounds effectively containing only one nuclear spin species, this being the spin-$\frac{1}{2}$ P^{31}. The natural abundance of Mg^{25} and Zn^{67} amounts to 10 and 4%, respectively. At the same field, the Larmor frequencies of these isotopes are shifted to lower values by more than a factor of 6 with respect to the P^{31} resonance. AlP, on the other hand, is a two-spin species substance with P^{31} and Al^{27} occurring with natural abundances of 100%. In addition, Al^{27} possesses spin $\frac{5}{2}$ so that quadrupolar effects may not be excluded.

Mg_3P_2 exhibits a cubic anti-manganese-oxide (Mn_2O_3) structure.[29,30] The phosphorus atoms form a face centered cubic lattice with one-quarter of the magnesium atoms occupying the center of each $\frac{1}{8}$ cube removed according to a regular scheme. One may therefore distinguish between two kinds of phosphorus atoms occupying slightly different positions with respect to the magnesium sites. There are those phosphorus atoms (P_I) placed at the corners of the cube and those (P_{II}) at the centers of any cube face. In either position, each phosphorus atom is surrounded by six magnesium atoms arranged at the corners of a simple cube. The Mg-P_I distances are all the same with two magnesium atoms missing along any body diagonal. There are, on the other hand, three different Mg-P_{II} distances of which two agree within 3%. In this case two magnesium sites along any face diagonal of the cube are not occupied. The ratio P_I to P_{II} of these two varieties of phosphorus atoms is therefore 1 to 3.

The lattice structure of Zn_3P_2 is related to that of Mg_3P_2.[30,31] The phosphorus atoms again form a face centered cubic lattice and each phosphorus site is surrounded by six zinc atoms. The zinc atoms in Zn_3P_2,

[29] *Landolt-Bornstein, Zahlenwerte und Funktionen*, edited by K. H. Hellwege (Springer Verlag, Berlin, 1955), Band I, Teil 4.

[30] J. R. Van Wazer, *Phosphorus and Its Compounds* (Interscience Publishers Inc., New York, 1958), Vol. I.

[31] C. Gottfried and F. Schossberger, *Strukturberichte*, Band III 1933–35.

TABLE I. Electronegativity differences, lattice parameters, and lattice sums[a] for three metal phosphides with P^{31} taken as resonant nucleus. a is the cubic edge of the phosphorus-centered cubic lattice. The summation indices κ and l refer to like and unlike neighbors, respectively.

Compound	Electronegativity difference	a [Å]	$\sum_k r_{jk}^{-6}$	$\sum_l r_{jl}^{-6}$
$Mg_3P^{31}_2$	0.9	6.00_5	$115.6a^{-6}$	$99.65a^{-6}$
$Zn_3P^{31}_2$	0.5	5.73	$115.6a^{-6}$	$40.85a^{-6}$
AlP^{31}	0.6	5.42	$115.6a^{-6}$	$660.50a^{-6}$

[a] H. S. Gutowsky, J. Chem. Phys. **20**, 1472 (1955); J. E. Mayer, *ibid.* **1**, 327 (1933); J. E. Jones and A. E. Ingham, Proc. Roy. Soc. (London) **A107**, 636 (1925).

however, are displaced considerably from the centers of the surrounding and slightly deformed phosphorus tetrahedrons in contrast to Mg_3P_2, where the magnesium atoms are located at the centers of somewhat deformed phosphorus tetrahedrons. The deformation effects on the lattice arising from the zinc atoms are larger than those caused by the magnesium atoms.[32] As a consequence, the cubic symmetry of the Mg_3P_2 lattice type is lowered to tetragonal symmetry for the Zn_3P_2 structure characterized by two lattice parameters. The lattice constants of all compounds studied in the present work are listed in Table I.

AlP is one of the III–V intermetallic semiconductors which crystallize in the zinc-blend lattice type.[29,30] The aluminum as well as the phosphorus atoms occupy the sites of a face centered cubic lattice with one lattice relatively shifted with respect to the other by one-quarter along the body diagonal. Each phosphorus atom is located in the center of an aluminum tetrahedron and, conversely, each aluminum atom exhibits tetrahedral coordination with respect to the phorphorus species. The lattice structure of metallic aluminum is face centered cubic.

The bonding in these metal phosphides is ionic-covalent. The ionic component formally contributes of the order of 25%.[33] In addition, however, charge separation effects arising from electronegativity differences between the various constituents have to be considered. As indicated in Table I, the electronegativity differences of the constituents in Zn_3P_2 and AlP are of the same order and smaller than in Mg_3P_2.[34] The last-named substance is therefore expected to exhibit a larger percentage of ionic bonding than the former materials. It has indeed been established that AlP and Zn_3P_2 have semiconducting properties while Mg_3P_2 shows a much lower conductivity.[30,35,36]

The theoretical and experimentally measured second moments of the samples studied are listed in Table II. For a sample containing two magnetically active nuclear species A and B the second moment of a dipolar broadened line in the crystalline powder average is given by[13]

$$\sigma_A^2=\sigma_{AA}^2+\sigma_{AB}^2=(3/5)\gamma_A^4\hbar^2 I_A(I_A+1)\sum_k r_{jk}^{-6}$$
$$+(4/15)\gamma_A^2\gamma_B^2\hbar^2 I_B(I_B+1)\sum_l r_{jl}^{-6}. \quad (39)$$

TABLE II. Calculated and measured root-mean-square second moments and transverse relaxation times $T_2(0)=1/\sigma_A$ of the static compounds studied. The atomic-mass superscript designates the resonant nucleus A of the compound.

Compound	$\sigma_{AA}/2\pi$ [kc/sec]	$(\sigma_A/2\pi)_{\text{calc}}$ [kc/sec]	$(\sigma_A/2\pi)_{\text{expt}}$ [kc/sec]	$T_2(0)$ [μsec]
$Mg_3P^{31}_2$	0.66	0.86	0.88	181
$Zn_3P^{31}_2$	0.75	0.91	1.02	156
AlP^{31}	0.89	4.00	3.10	51
$Al^{27}P$	1.26	2.17	2.80 1.90	57 84
Al^{27}	3.07	3.07	3.94	40

Here, the subscript A refers to the resonant species with gyromagnetic ratio γ_A and spin I_A and, similarly, for the second nuclear variety B. r_{jk} and r_{jl} denote the distances from the jth nucleus to its like and unlike neighbors, respectively.

In evaluating the inverse sixth-power internuclear distance summations, it has been assumed for simplicity that Mg_3P_2 and Zn_3P_2 crystallize in the anti-CaF_2 lattice type. The metal atoms then form a simple cubic lattice with 6/8 atom per unit cell and all phosphorous sites are equivalent. In addition, the isotopic abundance enters linearly into the lattice sum. The results are given in column 4 of Table I.

The P^{31} resonance signals of the polyscrystalline metal phosphides decay in a nearly Gaussian fashion. The P^{31} linewidths in Mg_3P_2 and Zn_3P_2 are entirely generated by nuclear dipolar broadenings with the non-resonant metal nuclei contributing 23 and 18%, respectively, to the total line breadths. The Gaussian decay of the Al^{27} resonance in aluminum metal is modified by the occurrence of a "Lowe beat"[15] and the observed root-mean-square second moment of the powdered sample is larger than its calculated value. This agrees with previously reported observations[37] and probably arises from quadrupolar broadening. A quadrupole echo[38] has been observed with the present aluminum sample which had an average particle size of 5 μ.

The situation with regard to AlP appears to be quite complex. The observed linewidth of the P^{31} resonance is smaller than its calculated value. The Al^{27} resonance cannot be described by a simple line-shape function. When the induction decay is approximated by two

[32] M. von Stackelberg and R. Paulus, Z. Physik. Chem. (B) **28**, 427 (1935).
[33] C. H. L. Goodman, Nature **187**, 590 (1960).
[34] L. Pauling, *The Nature of the Chemical Bond* (Cornell University Press, Ithaca, New York, 1960), 3rd ed.
[35] J. Lagrenaudie, J. Phys. Radium **17**, 359 (1956).
[36] H. G. Grimmeiss, W. Kischio, and A. Rabenau, J. Phys. Chem. Solids **16**, 302 (1960).
[37] J. J. Spokas and C. P. Slichter, Phys. Rev. **113**, 1462 (1959).
[38] I. Solomon, Phys. Rev. **110**, 61 (1958).

Gaussians, the root-mean-square second moment of the initial part of the decay is larger and that of the main part is smaller than the calculated value obtained solely on the basis of magnetic dipolar contributions to the linewidth. A first-order quadrupole broadening of the Al^{27} line is confirmed by the existence of an Al^{27} quadrupolar echo in the static sample. The nature of the line narrowing mechanism of both the P^{31} and Al^{27} resonance signals in this compound is not well understood. Atomic diffusion is unlikely to be significant at 300°K. The melting point of AlP is above 1700°C.[30] A line broadening of the resonance of either constituent is usually observed in other III–V compounds arising from indirect exchange among nonequivalent nuclei.[39–41] In contrast to these solids, however, there exists in AlP only one isotope of either constituent. Bound electrons cannot be responsible for the observed exchange narrowing in AlP since the nearest neighbors of any nuclear spin are members of the other species. No information about the impurity content of the present sample is available so that the structure of possible impurity levels is not known.

B. Transverse Relaxation

The variation of the transverse relaxation time $T_2(\Omega)$ of the P^{31} resonance in Mg_3P_2 as a function of the frequency Ω of sample rotation at the magic angle is shown in Fig. 3. The experimental arrangement of the rotor suspension did not permit taking reliable data below 2 kc/sec. A linear extrapolation of the experimental data toward zero frequency results in a value of $T_2(0)$ much larger than was found for the static sample (Table II). The stochastic theory of a rotating solid predicts $T_2(\Omega) \propto \Omega^2$ for $\sigma/\Omega \lesssim 1$ [Eq. (19)]. In the region between 2 and about 5 kc/sec, however, $T_2(\Omega)$ was found to vary linearly with Ω in disagreement with (19). One is rather reminded of the case of random motion where the inverse linewidth is linearly proportional to the correlation frequency.

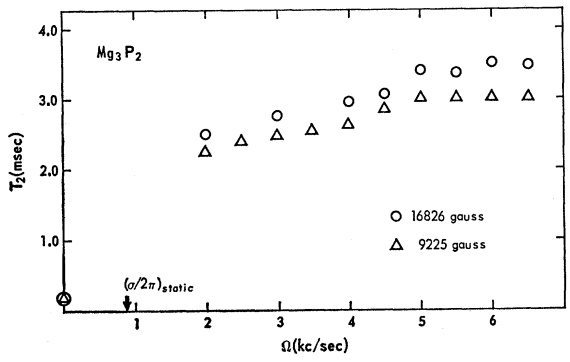

FIG. 3. Dependence of the P^{31} transverse relaxation time in Mg_3P_2 on the frequency of sample rotation.

In a rigid lattice the correlation time τ_c is the average time between simultaneous energy conserving transitions of two or more neighboring nuclear spins. It characterizes the rate at which spin diffusion can proceed in a solid and should depend on Ω as discussed in Sec. II B. Instead of (13), we choose a more rapidly decaying correlation function which from (14) and at the magic angle takes on the form

$$\langle \Delta\omega(t)\Delta\omega(t-\tau)\rangle = \tfrac{1}{3}\sigma^2 e^{-(\sigma+\Omega)\tau/\sigma\tau_c}(2\cos\Omega\tau+\cos 2\Omega\tau). \quad (40)$$

Equation (40) properly reduces to the correlation function of the static sample for $\Omega/\sigma \ll 1$. With (9), the inverse linewidth $T_2(\Omega)$ of a rotating solid is then immediately obtained for $\Omega/\sigma \gg 1$:

$$\Phi_\Omega(t) \approx \exp\left\{-\tfrac{1}{3}\sigma^2 t\int_0^\infty e^{-\Omega\tau/\sigma\tau_c}(2\cos\Omega\tau+\cos 2\Omega\tau)d\tau\right\}$$
$$= \exp\{-t/T_2(\Omega)\}, \quad (41)$$

with

$$T_2(\Omega) = \tfrac{4}{3}\Omega\tau_c/\sigma,$$

which is the desired relationship between $T_2(\Omega)$ and Ω in the region where $T_2(\Omega) \propto \Omega$.

The experimental data in Fig. 3 indicate that the phosphorus $T_2(\Omega)$ in Mg_3P_2 may become independent of Ω above 5 kc/sec. A 90°–180° pulse sequence did not produce a spin echo under these conditions. If the transverse relaxation time is rotationally invariant for $\Omega/\sigma \gg 1$, the dominant interaction between the nuclear spins causing line broadening cannot depend on the internuclear vector. It has to be invariant under rotation and hence must be expressible as a scalar product of nuclear spin operators. It seems reasonable to conclude that the ultimate width $1/T_2(\infty)$ of the Lorentzian-shaped line of the P^{31} resonance in Mg_3P_2 is determined by an indirect exchange coupling between dissimilar P^{31} nuclei (Sec. IV A and Fig. 8) with characteristic frequency $J' = 1/T_2(\infty) \cong 290$ cps.

A similar analysis for the P^{31} resonance in Zn_3P_2 cannot be given since the signal was inhomogeneously broadened by the variation of the external magnetic field along the axis of rotation. However, it could be established from spin echoes (Fig. 7) that $T_2(\Omega) \geq 20$ msec at 5 kc/sec. The line has thus been rotationally narrowed by about a factor of 130. If $T_2(\Omega)$ of the P^{31} resonance in this compound does also become invariant under rotation for $\Omega/\sigma \gg 1$, the indirect exchange frequency between nonequivalent P^{31} nuclei (Sec. IV A and Fig. 9) must be $J' \leq 50$ cps.

The transverse relaxation times of the Al^{27} resonances in AlP and aluminum metal as a function of the frequency of rotation at the magic angle are plotted in Fig. 4(a). The analysis of these data presents additional difficulties since these signals are broadened by quad-

[39] R. G. Shulman, J. M. Mays, and D. W. McCall, Phys. Rev. **100**, 692 (1955).
[40] R. G. Shulman, B. J. Wyluda, and H. J. Hrostowski, Phys. Rev. **109**, 808 (1958).
[41] M. J. Weber, J. Phys. Chem. Solids **21**, 210 (1961).

rupolar contributions which are also reduced by sample rotation.[11]

The Al^{27} decay in aluminum metal may be approximated as a Gaussian at frequencies $\Omega/\sigma<1$. At higher spinning frequencies a composite free induction signal is observed with a Gaussian initial part and a simple exponential tail. In this case, the time constant of the exponential decay is plotted in Fig. 4(a). After an approximately quadratic transition region, the T_2 data increase linearly with frequency. Since the linewidth of the static sample is quite large in comparison with the highest applied rotation frequency, the signal could be narrowed by only a factor of 10.

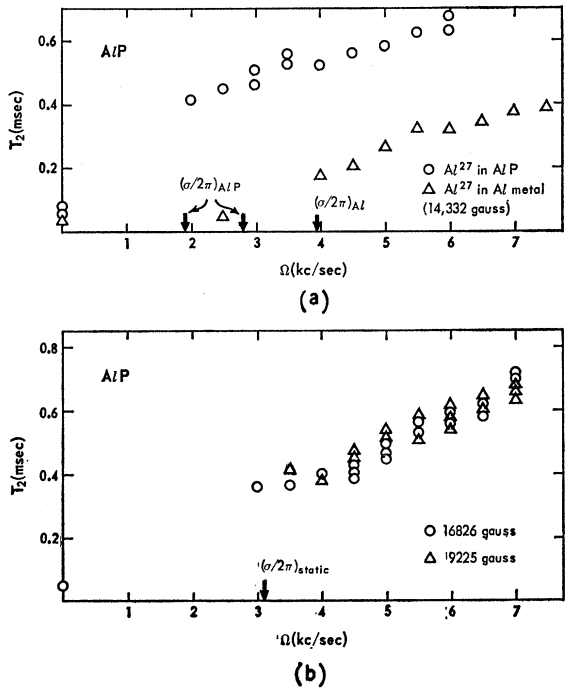

FIG. 4(a). Dependence of the Al^{27} transverse relaxation time in AlP (○) and Al metal (△) on the frequency of sample rotation. (b) Dependence of the P^{31} transverse relaxation time in AlP on the frequency of sample rotation.

The Al^{27} resonance signal of the static AlP sample is a composite decay broadened mainly by first-order quadrupole contributions and by the phosphorus nearest neighbors via the dipole-dipole coupling. The latter broadening amounts to about 30% in the static sample (Table II). At spinning frequencies above 3 kc/sec the Al^{27} free induction signals decay exponentially (Fig. 5) with time constants shown in Fig. 4(a). 90°–180° pulse sequences applied to the rotating sample do not produce spin echoes indicating that the static dipolar broadenings arising from neighboring phosphorus nuclei have been removed by rotation.

The magic angle $T_2^P(\Omega)$ values of the P^{31} resonance in AlP are plotted in Fig. 4(b) for two values of the applied magnetic field. In each case the data may be

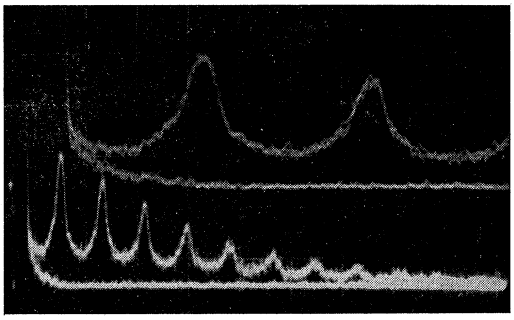

FIG. 5. Al^{27} free induction decay in AlP. The photograph is a superposition of three sweeps of signals from the static ($\Omega=0$) and rotating ($\Omega=6$ kc/sec) sample. Oscilloscope sweep rates: 50 μsec/division (upper beam), 200 μsec/division (lower beam).

represented by a straight line. The P^{31} signal again undergoes a transition from a Gaussian (static sample) to a simple exponential decay for frequencies $\Omega/\sigma\gtrsim1$. The presence of spin echoes shows that the P^{31} line is inhomogeneously broadened. Since the time constant due to the external field gradient across the rotating sample is large compared to the observed $T_2^P(\Omega)$ values it is probable that the inhomogeneous broadening arises from nearest-neighbor aluminum spins. The contribution of the Al^{27} nuclear spins amounts to about 70% of the root-mean-square second moment of the P^{31} line in static AlP (Table II). By varying the pulse separation of 90°–180° pulse sequences, the phosphorus-phosphorus transverse relaxation time $T_2^{P-P}(\Omega)$ has been determined at two spinning frequencies from the exponentially decaying envelope of the spin echoes; $T_2^{P-P}(\Omega)$ amounts to 1.20 msec and 1.64 msec at 5 and 6 kc/sec, respectively. A comparison with the total phosphorus transverse relaxation time $T_2^P(\Omega)$ in Fig. 4(b) at corresponding rotation frequencies shows that the contribution $T_2^{P-Al}(\Omega)$ of the aluminum nuclear spins to $T_2^P(\Omega)$ is attenuated by rotation in the same proportion as $T_2^P(\Omega)$ over the region tested, i.e.,

$$1/T_2^P(\Omega)=1/T_2^{P-P}(\Omega)+1/T_2^{P-Al}(\Omega), \quad (42)$$

where, within experimental accuracy $1/T_2^{P-Al}(\Omega)=0.65/T_2^P(\Omega)$. Hence, at frequencies $\Omega/\sigma\gtrsim1$ the aluminum spins still contribute about 65% to the local field at a phosphorus site while the phosphorus nuclei do not broaden the aluminum signal appreciably.

Owing to its smaller second moment in the static sample, the Al^{27} resonance in AlP is narrowed more rapidly initially than the P^{31} line (Table II and Fig. 4). In the following linear region, however, $T_2^{Al}(\Omega)$ increases at a smaller rate than $T_2^P(\Omega)$. The electric quadrupolar broadening of the Al^{27} line in AlP (and metallic aluminum) apparently is not reduced as effectively by rotation as the magnetic dipolar contributions.

C. Chemical Shift

For spinning frequencies at which the magnetic dipolar coupling is sufficiently reduced, the P^{31} reso-

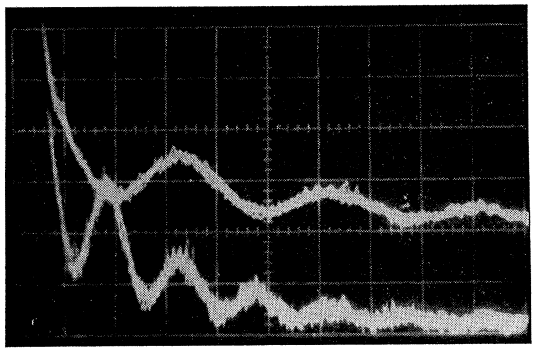

FIG. 6. P^{31} free induction decay in Mg_3P_2. The photograph is a superposition of five sweeps. $\omega_0/2\pi=29.0$ Mc/sec and $\Omega=6$ kc/sec. Oscilloscope sweep rates: 0.5 msec/division (upper beam), 1.0 msec/division (lower beam).

nance signals observed in Mg_3P_2 and Zn_3P_2 exhibit a fine structure (Figs. 6 and 7). In each case the additional modulation frequency is proportional to the external field and therefore has to be attributed to the existence of at least two groups of nonequivalent phosphorus nuclei located in different chemical environments of the crystal.

Since the chemical shift pattern observed is very nearly periodic, it may be assumed that the chemical shift is large compared to any indirect exchange coupling that might be present among dissimilar spins in the solid.[42] Anticipating an exponential decay of the nuclear signal (18) with time constant $T_2(\Omega)$, the normalized x component of magnetization for M groups of nonequivalent spin-$\frac{1}{2}$ phosphorus nuclei may be shown to be[11]

$$\Phi_\Omega(t)=\frac{M_x(t)}{M_x(0)}=\frac{e^{-t/T_2(\Omega)}}{N\gamma_0^2}\sum_{k=1}^{M}N_k\gamma_k^2\cos\omega_k t, \quad (43)$$

where $N=\sum_{k=1}^{M}N_k=$ total number of resonant spins, $N_k=$ number of spins in the kth group, $\omega_k=\gamma_k H_0=\omega_0+\delta_k$ with chemical shift $\delta_k\ll\omega_0, \omega_k$.

The analysis of the lattice structures of Mg_3P_2 and Zn_3P_2 shows (Sec. II A) that there are two groups of nonequivalent phosphorus nuclei in either compound.

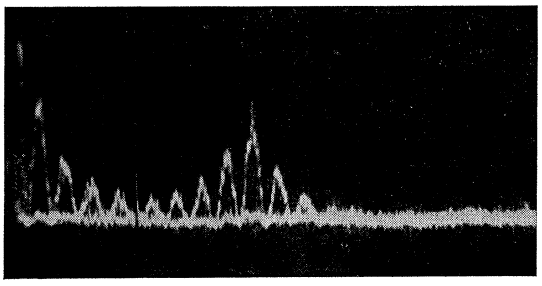

FIG. 7. P^{31} free induction decay and spin echo following 90°–180° pulse sequence in Zn_3P_2. $\omega_0/2\pi=29.0$ Mc/sec and $\Omega=5$ kc/sec. Oscilloscope sweep rate: 2.0 msec/division.

[42] E. L. Hahn and D. E. Maxwell, Phys. Rev. 88, 1070 (1952).

Since only the relative chemical shift δ between these two groups can be determined from the present data and not the exact positions of the fine-structure lines within the dipolar broadened signal of the static sample, one can center one of the lines at the average Larmor frequency ω_0. Neglecting terms in $\delta/\omega_0\lesssim 3\times10^{-5}$, (43) reduces to

$$\Phi_\Omega(t)=F(t)\cos\omega_0 t-G(t)\sin\omega_0 t, \quad (44)$$

where

$$F(t)=(N_1/N)[(N_0/N_1)+\cos\delta t]e^{-t/T_2(\Omega)},$$

$$G(t)=(N_1/N)\sin\delta t\, e^{-t/T_2(\Omega)},$$

and

$$N=N_0+N_1.$$

The Fourier transform of (44) corresponding to the absorption line shape[14,15] is found to be

$$\Gamma(\Delta\omega)=\frac{T_2(\Omega)}{N\pi}\left\{\frac{N_0}{1+[\Delta\omega T_2(\Omega)]^2}+\frac{N_1}{1+[(\Delta\omega+\delta)T_2(\Omega)]^2}\right\}, \quad (45)$$

which is simply the sum of two Lorentzian functions centered at $\Delta\omega=\omega-\omega_0=0$ and $-\Delta\omega=\delta$, respectively, each one being weighted by the normalized number of spins contained in each respective group.

Equation (44) may be rewritten as

$$\Phi_\Omega(t)=[F(t)^2+G(t)^2]^{1/2}\times\cos\{\omega_0 t+\tan^{-1}[G(t)/F(t)]\}. \quad (46)$$

In an incoherent transient experiment the rf free precession signal is demodulated, i.e., rectified and passed through a low-pass filter. Only its envelope $R(t)=[F(t)^2+G(t)^2]^{1/2}$ is therefore observed rather than $F(t)$ or $G(t)$ separately. The detected free induction decay of a chemically shifted doublet is then given by

$$R(t)=(N_1/N)[1+(N_0/N_1)^2+2(N_0/N_1)\cos\delta t]^{1/2}e^{-t/T_2(\Omega)}. \quad (47)$$

In particular, the observed P^{31} free induction decay in Mg_3P_2 with $N_0=3N_1$, is predicted to be

$$R(t)=\tfrac{1}{4}[10+6\cos\delta t]^{1/2}e^{-t/T_2(\Omega)}. \quad (48)$$

The experimentally determined values of the relative chemical shift $\delta/\omega_0=24$ ppm and of the transverse relaxation time $T_2=3.5$ msec at $\Omega=6.0$ kc/sec (at which T_2 from Fig. 3 appears to be independent of Ω) have been used to evaluate (48). The result is plotted in Fig. 8(a) and compared with the observed P^{31} signal in Mg_3P_2 at $\omega_0/2\pi=29.0$ Mc/sec. Also shown in Fig. 8(a) is the Gaussian P^{31} decay of the static sample with root-mean-square second moment $\sigma=5.53\times10^3$ rad/sec (from Table II). The corresponding P^{31} absorption line shapes of the static and rotating Mg_3P_2 sample have been calculated and plotted in Fig. 8(b).

In order to fit an expression of the form (47) to the

observed P^{31} free induction decays of a rapidly rotating sample of Zn_3P_2, it has to be assumed that two groups of nonequivalent phosphorus nuclei exist in this solid, each one containing an identical number of spins, i.e., $N_0=N_1$. One then obtains from (47)

$$R(t)=(\cos\tfrac{1}{2}\delta t)e^{-t/T_2(\Omega)}. \qquad (49)$$

Equation (49) has been plotted in Fig. 9(a) using $\delta/\omega_0=35$ ppm and $T_2=3.35$ msec (at $\Omega=5.0$ kc/sec) from experiment. It is being compared with the experimentally observed P^{31} decay in Zn_3P_2 obtained at $\Omega=5.0$ kc/sec and $\omega_0/2\pi=29.0$ Mc/sec. The corresponding absorption line shape has been evaluated using (45) and is shown in Fig. 9(b) together with the Fourier transform of the nearly Gaussian P^{31} free induction decay of that static solid with $\theta=6.41\times10^3$ rad/sec. It should be noted that both the free precession signal and the absorption line of the rotating Zn_3P_2 sample are inhomogeneously broadened by the action of the external magnetic field. They should be narrower by at least a factor of 6 as indicated by spin-echo measurements (Fig. 7).

D. Lontitudinal Relaxation

Two samples of Mg_3P_2 with different impurity concentrations were available. The longitudinal relaxation

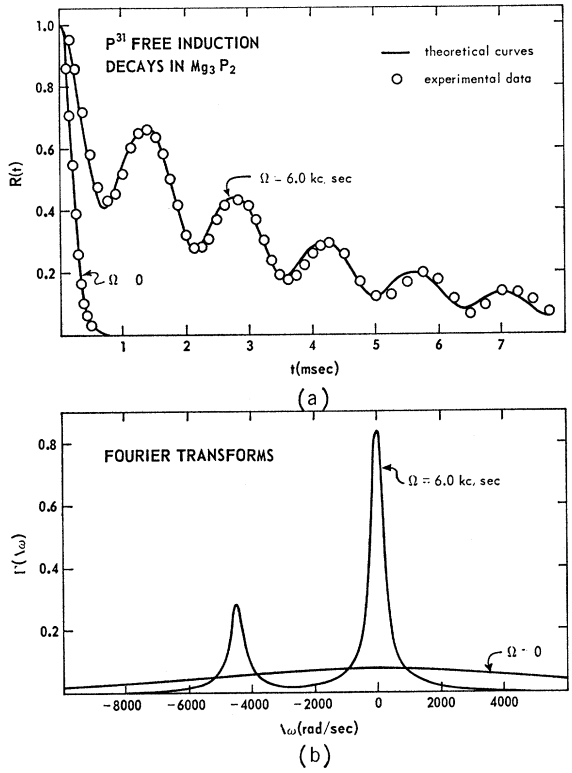

FIG. 8. Normalized P^{31} free induction decays for a static ($\Omega=0$) and rotating sample ($\Omega=6.0$ kc/sec) of Mg_3P_2 and their Fourier transforms at $H_0=16826$ G.

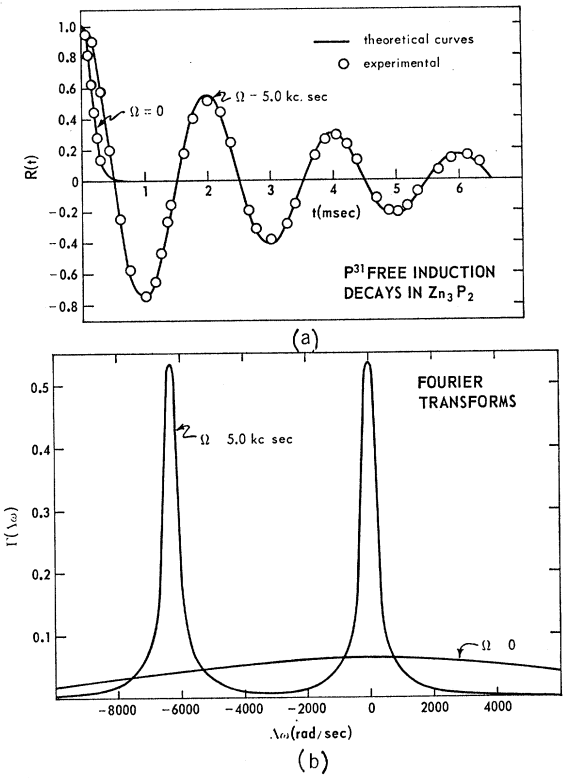

FIG. 9. Normalized P^{31} free induction decays for a static ($\Omega=0$ kc/sec) and rotating sample ($\Omega=5.0$ kc/sec) of Zn_3P_2 and their Fourier transforms at $H_0=16826$ G.

times $T_1(H_0,0)$ of the P^{31} nuclei in the static solids differ by more than two orders of magnitude. The magnetization recovery in sample (A) proceeds at an exponential rate for all spinning frequencies. The resultant values of $T_1(H_0,\Omega)$ are of the order of several seconds and depend linearly on H_0 for fixed Ω. This behavior is characteristic for rapid-diffusion relaxation with $\omega_I\tau_e\ll1$, where τ_e is the electronic relaxation time and ω_I the nuclear Larmor precession frequency.[22]

The P^{31} magnetization recovery of sample (B) of Mg_3P_2 and of Zn_3P_2 is of a composite nature. After a transition region for short times following initial saturation of the spin system, the recovery approaches exponential growth for longer waiting times τ. The associated values of $T_1(H_0,\Omega)$ for either solid taken from the exponential portion of the curves are of the order of several hundred seconds and, within experimental accuracy, increase as $H_0^{1/2}$ for constant Ω. These measurements indicate that the P^{31} nuclear relaxation is diffusion-limited with $\omega_I\tau_e\gg1$. An example of this case is provided in Fig. 10 in which the fractional magnetization recovery of P^{31} in Zn_3P_2 is plotted for various Ω.

The poor signal-to-noise ratio of the small rotor samples did not permit a detailed analysis of the time dependence of the transition region in the magnetization recovery and its modification under sample rotation. Blumberg[22] proposes that the magnetization grows as

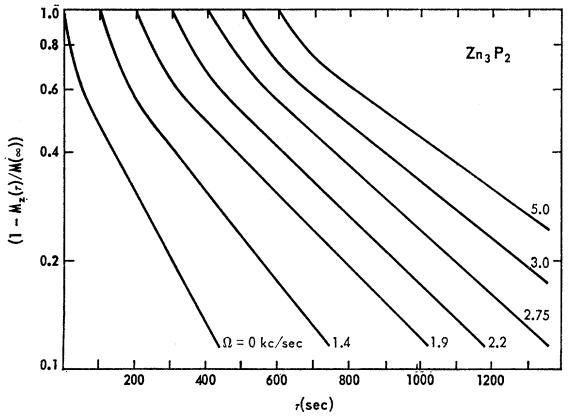

FIG. 10. Nuclear magnetization recovery of P^{31} in Zn_3P_2 at various spinning frequencies in kc/sec and $H_0=9225$ G. The abscissa has been shifted by 100 sec for successive spinning frequencies to separate the curves.

$\tau^{1/2}$ for short waiting times τ after initial saturation. Other investigations[43] show that a compound recovery arises if more than one time constant are present in the approach of the spin system toward thermal equilibrium. Both interpretations of the transition region assume that a non-negligible number of nuclei experience the influence of only one or very few impurity ions during relaxation. This phenomenon may be called localized relaxation. The majority of nuclear spins, on the other hand, reaches a common spin temperature via spin diffusion such that each bulk nucleus "sees" a large number of paramagnetic ions in the course of relaxation. Depending upon the contribution of an impurity ion to the local field at a nuclear site, one would expect the Larmor frequencies of the nuclei in the region of localized relaxation to be shifted into the wings of the resonance absorption line, if observable at at all.[23,44] The center portion of the line then has to be attributed to the resonance response of the bulk nuclei.

This statement can be tested experimentally since the observed P^{31} free induction decays in Mg_3P_2 and Zn_3P_2 are expanded by at least one order of magnitude by sample rotation at the magic angle. It was found consistently that the transition region in diffusion-limited relaxation could be detected only if the family

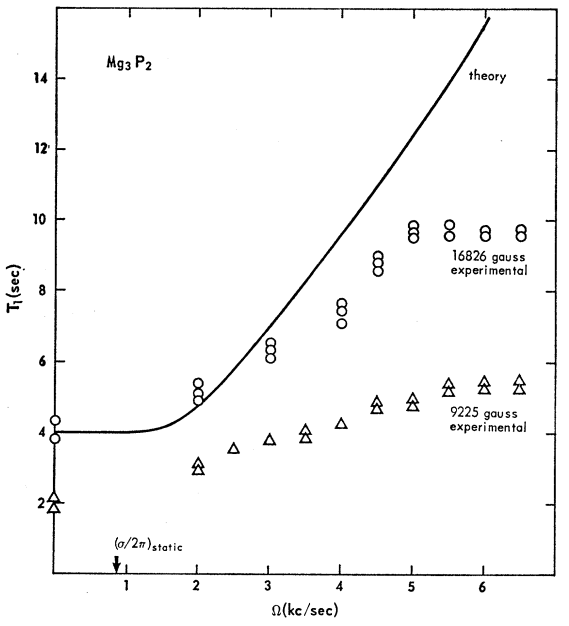

FIG. 11. Dependence of the P^{31} longitudinal relaxation time in Mg_3P_2 on the frequency of sample rotation at two different values of the external field. The theoretical curve has been obtained for $\Omega/\sigma>1$ by assuming only dipolar couplings among the nuclei.

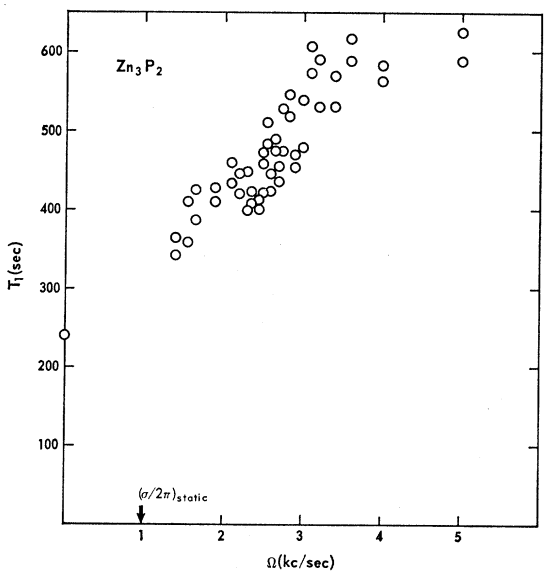

FIG. 12. Dependence of the P^{31} longitudinal relaxation time in Zn_3P_2 on the frequency of sample rotation at $H_0=9225$ G.

of free induction decays representing the magnetization recovery was analyzed at a fixed time $t\lesssim T_2(0)$ after application of the sampling 90° pulse at which rapidly dephasing nuclear spins still contribute to the signal. For sufficiently large t, the magnetization recovery is governed by a single exponential with time constant equal to the limiting T_1 in the compound recovery. It is this time constant that has been determined as a function of Ω.

The dependence of the longitudinal relaxation time $T_1(H_0,\Omega)$ of the P^{31} bulk nuclei in sample (A) of Mg_3P_2 and in Zn_3P_2 on the frequency Ω of sample rotation at the magic angle is shown in Figs. 11 and 12, respectively. $T_1(H_0,\Omega)$ increases with increasing $\Omega/\sigma\gtrsim 1$ in both compounds as predicted by the stochastic theory of spin

[43] J. R. Gaines, K. Luszczynski, and R. E. Norberg, Phys. Rev. 131, 901 (1963).

[44] G. R. Khutsishvili, Zh. Eksperim. i Teor. Phys. 43, 2179 (1962) [English transl.: Soviet Phys.—JETP 16, 1540 (1963)].

TABLE III. Characteristic ratios of the static ($\Omega=0$) and rotationally invariant ($\Omega\to\infty$) values of the P^{31} longitudinal relaxation time $T_1(H_0,\Omega)$ in Zn_3P_2 and in two Mg_3P_2 samples. The ratio of the applied magnetic fields is $H_1/H_2=1.82$.

Compound	$\omega_0/2\pi$ (Mc/sec)	$T_1(H_0,0)$ (sec)	$T_1(H_0,\infty)$ (sec)	$\frac{T_1(H_0,\infty)}{T_1(H_0,0)}$	$\frac{T_1(H_1,0)}{T_1(H_2,0)}$	$\frac{T_1(H_1,\infty)}{T_1(H_2,\infty)}$
Mg_3P_2 (A)	29.0	4.0	9.7	2.4	2.0	1.8
	15.9	2.0	5.3	2.6		
Mg_3P_2 (B)	29.0	640	1550	2.4	1.5	...
	15.9	430	...	...		
Zn_3P_2	15.9	240	600	2.5	...	...

diffusion (Sec. II B). The magnetic dipole-dipole interaction between the nuclear spins is reduced by mechanical rotation of the specimen causing spin diffusion to be less effective in producing equilibrium among the nuclei and in transporting spin energy toward impurity centers. In addition, the phosphorus T_1 in sample (B) of Mg_3P_2 has been measured in the static and rapidly rotating specimen with results listed in Table III. The observed variation of $T_1(H_0,\Omega)$ with Ω appears to be identical in the two Mg_3P_2 samples. At constant H_0, one curve is simply shifted with respect to the other by the ratio of the respective static T_1 values.

$T_1(H_0,\Omega)$ of the P^{31} nuclei in Mg_3P_2 as a function of Ω has been calculated from (37) and (32) using the measured values of σ (Table II) and $T_2(\Omega)$ (Fig. 3). The resulting curve is fitted to $T_1(H_0,0)$ for sample (A) of Mg_3P_2 at $H_0=16\,826$ G and plotted in Fig. 11. No satisfactory fit can be claimed. In particular, the experimental data become independent of Ω at higher spinning frequencies, between 5.0 and 5.5 kc/sec in Mg_3P_2 and above 4.0 kc/sec in Zn_3P_2. In Mg_3P_2, this transition occurs at approximately the same Ω at which $T_2(\Omega)$ also becomes invariant under sample rotation (Fig. 3). This behavior suggests that in Mg_3P_2 rotated at 5 kc/sec and above, the nuclear dipolar interaction or, for that matter, any rotationally noninvariant interaction present among the nuclei, becomes negligible and ineffective in producing line broadening as well as spin diffusion.

The ratio $T_1(H_0,\infty)/T_1(H_0,0)$ of the rotationally invariant to the static value of the longitudinal relaxation time $T_1(H_0,\Omega)$ is within experimental accuracy equal to 2.5 in both Mg_3P_2 and Zn_3P_2 (Table III) independent of the effective impurity density and applied magnetic field (for Mg_3P_2). One therefore has with reference to Eq. (37)

$$D(\infty)/D(0)=0.3, \tag{50}$$

i.e. the spin-diffusion constant $D(\Omega)$ could be reduced by about a factor of 3 by rapidly rotating these compounds at the magic angle.

The invariance of $T_1(H_0,\Omega)$ at high Ω implies that spin diffusion in Mg_3P_2 and Zn_3P_2 is ultimately sustained by an interaction between the spin-$\frac{1}{2}$ P^{31} nuclei other than the magnetic dipolar coupling. Obviously, this interaction itself has to be invariant under rotation and hence cannot depend on the spatial coordinates of the nuclear spins. It is reasonable to speculate that an indirect nuclear exchange coupling of the form

$$\mathcal{H}_{cx}=\hbar\sum_{j<k}J_{jk}\mathbf{I}_j\cdot\mathbf{I}_k \tag{51}$$

is responsible for establishing equilibrium among the nuclei in a rapidly rotating sample of Mg_3P_2 or Zn_3P_2.

The spin-diffusion calculation for a rotating solid presented in Sec. II B is strictly based on a dipolar model. It has to be modified if exchange effects are to be included. The transition probability W_{jk} per unit time for a simultaneous spin flip of an antiparallel nuclear pair to occur is then determined by

$$W_{jk}=2\pi\hbar^{-1}|\langle\alpha'|G_{jk}^{(0)}(t)+\mathcal{H}_{jk}^{ex}|\alpha\rangle|^2 \times\rho(E_{\alpha'})\delta(E_{\alpha'}-E_\alpha), \tag{52}$$

where $G_{jk}^{(0)}(t)$ and $\mathcal{H}_{jk}^{ex}$ represent the contributions of dipolar and exchange coupling and are given by Eqs. (28) and (51), respectively. The density $\rho(E_{\alpha'})$ of final states may be replaced by an integral over the frequency distributions of the jth and kth nuclear spin which are assumed to be represented by the line-shape function. Invoking the Fourier transform theorem (30), the total transition probability $W(\Omega)$ per unit time is then obtained from (31) and (52) by summing over all nuclei. At zero spinning frequency

$$W(0)=2\pi\sum_{j<k}[(\tfrac{1}{4}\gamma^2\hbar r_{jk}^{-3})^2(1-3\cos^2\vartheta_{jk})^2+J_{jk}^2] \times\int_{-\infty}^{\infty}\phi_0^2(t)dt \tag{53}$$

while for sufficiently large Ω at the magic angle

$$W(\infty)=2\pi\sum_{j<k}J_{jk}^2\int_{-\infty}^{\infty}\phi_\infty^2(t)dt. \tag{54}$$

The free induction decays $\Phi_0(t)$ of the static samples of the two metal phosphides are very nearly Gaussian. The second moment of the resonance absorption line of a single crystal containing only spin-$\frac{1}{2}$ nuclei is given by[13]

$$1/T_2^2(0)=9\sum_k(\tfrac{1}{4}\gamma^2\hbar r_{jk}^{-3})^2(1-3\cos^2\vartheta_{jk})^2.$$

If the angular dependence of the internuclear interaction

is neglected, the spin diffusion coefficient $D(\Omega)$ may be defined as $D(\Omega)=a^2W(\Omega)$[12], where a is the cubic edge of the lattice. In the limit of zero and sufficiently large spinning frequencies, $D(\Omega)$ then becomes with Eqs. (53) and (54)

$$D(0)=2\pi\sqrt{\pi}a^2T_2(0)[\tfrac{1}{9}T_2^{-2}(0)+J^2],$$
$$D(\infty)=2\pi a^2J^2\int_{-\infty}^{\infty}\Phi_\infty^2(t)dt. \quad (55)$$

If the chemical shift modulation of the free precession signals is omitted for the moment, i.e., $\Phi_\infty(t)=\exp[-t/T_2(\infty)]$ for sufficiently large Ω, the exchange frequency J from (55) is determined by

$$J^2=\frac{(\pi)^{1/2}}{9T_2(0)T_2(\infty)}\frac{D(\infty)}{D(0)}\times\left[1-(\pi)^{1/2}\frac{D(\infty)}{D(0)}\frac{T_2(0)}{T_2(\infty)}\right]^{-1}. \quad (56)$$

On substituting numerical values for Mg_3P_2 into (56), $D(\infty)/D(0)=0.3$ [from (50)] and $T_2(0)/T_2(\infty)\cong 1/20$ (from Fig. 3), one finds that the indirect exchange coupling contributes less than 3% to spin diffusion in the static sample. For Zn_3P_2, this contribution should be even smaller.

The proposed model then asserts that at zero spinning frequency, spin diffusion in Mg_3P_2 and Zn_3P_2 is dominated by magnetic dipolar couplings while at frequencies at which $T_1(H_0,\Omega)$ is invariant under rotation, dipolar effects are negligible and indirect nuclear exchange maintains the process of spin diffusion. Equation (55) then determines the exchange frequency J as

$$J^2=\frac{(\pi)^{1/2}}{9}\frac{D(\infty)}{D(0)}\left[T_2(0)\int_{-\infty}^{\infty}\Phi_\infty^2(t)dt\right]^{-1}. \quad (57)$$

For Mg_3P_2 and Zn_3P_2, $D(\infty)/D(0)$ and $T_2(0)$ are given by Eq. (50) and Table II, respectively.

In addition, the rotationally invariant free induction decay $\Phi_\infty(t)$ is needed for a numerical evaluation of expression (57). $\Phi_\infty(t)$ has been observed for sufficiently large Ω only in Mg_3P_2. From Eq. (44) one obtains upon integration

$$\int_{-\infty}^{\infty}\Phi_\infty^2(t)dt=\left(\frac{N_1}{N}\right)^2T_2(\infty)\times\left[1+\left(\frac{N_0}{N_1}\right)^2+2\frac{N_0}{N_1}\frac{1}{1+[\frac{1}{2}\delta T_2(\infty)]^2}\right], \quad (58)$$

where the total number of spins $N=N_0+N_1$ with $N_0=3N_1$ for Mg_3P_2 and $N_0=N_1$ for Zn_3P_2. The measured values of $T_2(\infty)$ and δ/ω_0 are shown in Table IV, together with the J values calculated from (57) and (58).

TABLE IV. Rotationally invariant transverse relaxation time $T_2(\infty)$, relative chemical shift δ and exchange frequency J in Mg_3P_2 and Zn_3P_2.

Compound	$\omega_0/2\pi$ [Mc/sec]	$T_2(\infty)$ [sec]	δ/ω_0 [ppm]	J [cps]
Mg_3P_2	29.0	3.5×10^{-3}	24	340
	15.9			320
Zn_3P_2	29.0	$\geq 2\times10^{-2}$	35	$\leq$190
	15.9			$\leq$180

The exchange frequency J as defined by Eq. (57) is expected to be larger than the value J' obtained from the ultimate linewidth in rotating solids (Sec. IV B). J contains contributions from dissimilar and similar P^{31} nuclei since both contribute to spin diffusion. J furthermore depends on the strength of the applied magnetic field H_0 via the chemical shift δ in such a way that J increases with increasing H_0. For an infinite splitting ($\delta\to\infty$) of the doublet detected in these two metal phosphides, Eq. (57) predicts J to be larger by factors of $(8/5)^{1/2}$ and $\sqrt{2}$ in Mg_3P_2 and Zn_3P_2, respectively, than its corresponding values for $\delta=0$ where the two lines collapse into a single line.

The variation of $T_1(H_0,\Omega)$ with Ω at the magic angle of the P^{31} and Al^{27} nuclei in AlP is shown in Fig. 13. The magnetization recovery of the Al^{27} nuclei is observed to proceed according to a single exponential for all Ω's. The characteristic time constant of the recovery is equal to 18.5 sec and is invariant under rotation (Fig. 13). $T_2^{Al}(\Omega)$, on the other hand, increases linearly with Ω up to the highest applied spinning frequency (Fig. 4). The dominant relaxation process of the spin-$\frac{5}{2}$ Al^{27} nuclei is probably determined by a direct quadrupolar coupling to the lattice.[45,46] For spinning frequencies small compared to the Larmor precession, this relaxation process would be expected to be unaffected by spinning.

The longitudinal relaxation of the P^{31} nuclei in AlP displays some unusual features. T_1^P of the static sample is smaller than T_1^{Al} and appears to be directly proportional to H_0. The magnetization recovery curves display a pronounced transition region for all spinning frequencies. At both magnetic fields studied, $T_1^P(H_0,\Omega)$ increases with increasing Ω and it appears that the P^{31} nuclei relax (for zero and low spinning frequencies) to the impurity centers via spin diffusion. However, as $T_1^P(H_0,\Omega)$ approaches the constant value of T_1^{Al}, it becomes independent of Ω for either value of H_0 (Fig. 13), while $T_2^P(\Omega)$ continues to increase linearly with Ω up to the highest applied spinning frequency (Fig. 4).

These measurements suggest that the P^{31} longitudinal relaxation in this covalent solid is dominated at suffi-

[45] J. Van Kranendonk, Physica **20**, 781 (1954).
[46] E. R. Andrew, A. Bradbury, R. G. Eades, and V. T. Wynn, Phys. Letters 4, 99 (1963).

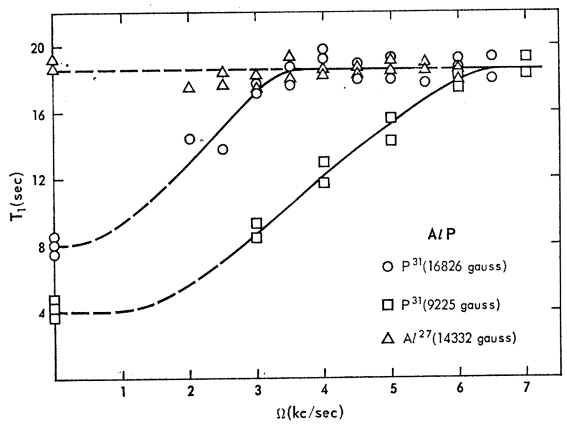

FIG. 13. Dependence of the P^{31} and Al^{27} longitudinal relaxation times in AlP on the frequency of sample rotation. The P^{31} data have been obtained at two values of the external field.

ciently large Ω by some indirect and rotationally invariant cross relaxation between the P^{31} and Al^{27} nuclear spins. However, no convincing model for such a process can be offered which would explain why the Al^{27} nuclei do not relax via the P^{31} spins at zero or low spinning frequencies if the reverse process should be possible at frequencies at which $T_1^P(H_0,\Omega)$ approaches T_1^{Al}. A cross-relaxation effect induced by specimen rotation described by Andrew *et al.*[46] in solid phosphorus pentachloride cannot be responsible for this behavior since the ratio of the P^{31} and Al^{27} gyromagnetic ratios is 1.55. It has been reported[41,47] that in the similar III–V compounds of GaP and InP, T_1^P is larger at room temperature by at least one order of magnitude than the longitudinal relaxation time of the Group III element. It is very likely that the impurity concentration in the present sample of AlP is so large that first-order quadrupole broadening of the Al^{27} resonance appears. Pronounced Al^{27} quadrupolar echoes have indeed been observed. Quadrupole broadening would further be accompanied by a reduction in the spin diffusion rate among the Al^{27} nuclei and (if enough of the impurities are paramagnetic) a short longitudinal relaxation time of the P^{31} spins, in accordance with the experimental results. The local fields at the P^{31} and Al^{27} sites are dominated by the aluminum nearest neighbors for all applied spinning frequencies (Sec. IV B).

[47] R. L. Mieher, Phys. Rev. **125**, 1537 (1962).

V. SUMMARY

Mechanical sample rotation at the magic angle has been used in determining the fine structure of the dipolar broadened lines of several metal phosphides. The resonance lines appear to narrow coherently (i.e., $T_2 \propto \Omega^2$) for spinning frequencies of the order of the static linewidth. For $\Omega/\sigma > 1$, however, only a linear increase of T_2 with Ω has been recorded. Two groups of nonequivalent P^{31} spins have been isolated in Mg_3P_2 and Zn_3P_2. In Mg_3P_2, and possibly in Zn_3P_2, both T_2 and T_1 become ultimately independent of rotation. It is then possible to determine the magnitude of the indirect nuclear exchange frequency between dissimilar as well as similar P^{31} nuclei. The results obtained by rotating AlP are only partially understood. Additional measurements on samples of this compound containing different paramagnetic impurity concentrations would be needed to ascertain cross relaxation among the constituents.

ACKNOWLEDGMENTS

The authors are indebted to Professor K. Luszczynski for many helpful suggestions regarding experimental procedure. Professor D. J. Scalapino of the University of Pennsylvania, Dr. B. Robertson of Cornell University, and Dr. M. Goldman of the Centre d'Etudes Nucleaires de Saclay, France, made several informative observations on theoretical aspects of the work. L. Shen assisted in several data runs and analysed some of the experimental results. Professor S. I. Weissman and S. E. Webber of the Washington University Chemistry Department prepared some of the metal phosphide samples. Dr. H. S. Jarrett of E. I. DuPont de Nemours & Company furnished several Delrin rods before they were commercially available. Most of the metal phosphides used in this investigation were obtained through the courtesy of Hooker Chemical Corporation, Niagara Falls, New York and Sigma Chemical Company, St. Louis, Missouri. The aluminum metal powder was furnished by Reynolds Metals Company.

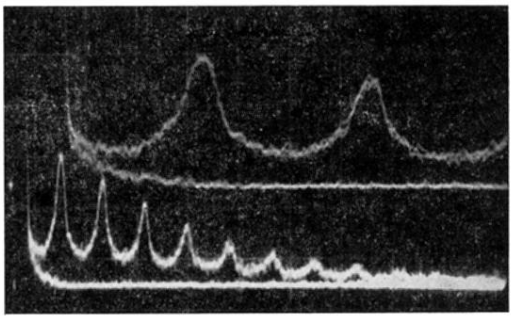

FIG. 5. Al^{27} free induction decay in AlP. The photograph is a superposition of three sweeps of signals from the static ($\Omega=0$) and rotating ($\Omega=6$ kc/sec) sample. Oscilloscope sweep rates: 50 μsec/division (upper beam), 200 μsec/division (lower beam).

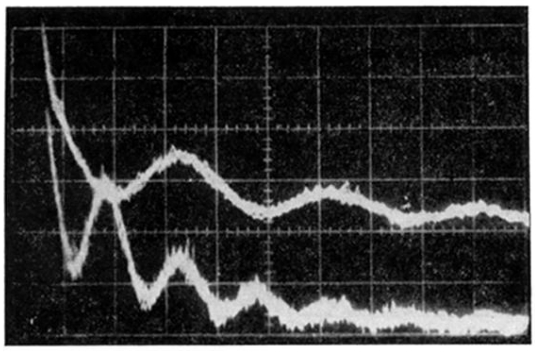

FIG. 6. P^{31} free induction decay in Mg_3P_2. The photograph is a superposition of five sweeps. $\omega_0/2\pi = 29.0$ Mc/sec and $\Omega = 6$ kc/sec. Oscilloscope sweep rates: 0.5 msec/division (upper beam), 1.0 msec/division (lower beam).

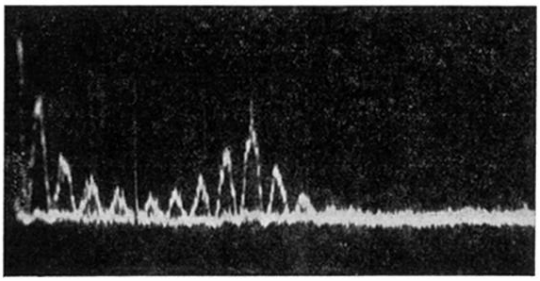

FIG. 7. P^{31} free induction decay and spin echo following 90°–180° pulse sequence in Zn_3P_2. $\omega_0/2\pi = 29.0$ Mc/sec and $\Omega = 5$ kc/sec. Oscilloscope sweep rate: 2.0 msec/division.